# Numerical modeling of induction assisted subsurface heating technology

By

Lei Zhang

A Thesis

Submit to the faculty of

WORCESTER POLYTECHNIC INSTITUTE

*In partial fulfillment of the requirements for the*

Degree of Master of Science

In

Manufacturing Engineering

By

_____

Feb 2012

APPROVED:

Yiming (Kevin) Rong, *Advisor*

*Associate Director* of Manufacturing and Materials Engineering

*Higgins Professor* of Mechanical Engineering

Richard D. Sisson Jr.

*Director* of Manufacturing and Materials Engineering

*George F. Fuller Professor*

Dean of Graduate Studies

# Abstract

Nickel-based super alloys are widely employed in the aerospace industry due to their high-temperature strength and high corrosion resistance. Because of the special application, the superficial residual stress of the super alloy is mandatory to 100% compressive stress according to the Federal Aviation Administration (FAA) regulations.

In manufacturing of nickel-based super alloy components, grinding processes are necessarily applied as the final material removal step for achieving the stringent tolerance and surface finish requirements. During the traditional grinding process of Nickel based alloy, due to the thermal effect, tensile residual stress might be generated on the surface of the alloy. It's critical to transfer the tensile residual stress to compressive one which benefits on the fatigue life of alloy.

In the thesis, a novel technology is developed to generate the superficial compressive residual stress with the method of embed a subsurface heating layer inside the workpiece to regulate the distribution of temperature field very before mechanical process. The residual stress might be reduced much, even transfer to compressive stress after combining the thermal effect.

The numerical model will be built in the thesis including the induction model, heat transfer model, grinding heat model. Effects of different parameters on final subsurface heating layer will be studied including the coil parameters, concentrator parameters, coolant parameters, feed rate and also electromagnetic field properties such as the skin effect, proximity effect and slot effect.

The thesis creates a system combining induction heating and cooling processes to regulate the temperature distribution in subsurface area that will be used for further stress analysis.

# Acknowledgement

It's my great pleasure to thank all the people who helped me during my thesis and research work. It's your help encouraging me to overcome difficulties and finally finish the thesis.

First of all, I would like to express my sincere appreciation to my advisor, Prof. Yiming (Kevin) Rong. His numerous suggestions and immense knowledge shorten my way of research and strengthen my confidence when I bogged down. He not only helps me how to solve problem and finish my thesis but also train my logic mind in research that will influence me much for my future work.

And I'd like to thank Prof. Sisson for his support, guidance and encouragements throughout my graduate studies. He teaches me a lot how to face the investigation and to deal with people.

I also thank Prof. Yan Wang for the enthusiastic service on the thesis committee.

I would also like to thank my colleagues, Dr. Liang He, Yang Ge, Zhanshu He. They contributes a lot on the thesis, it's my honor to work with them. I benefit a lot from the invaluable suggestions and discussions. I would also thank the program secretary, Ms. Sue Milkman who helps me out during my stay at WPI.

Finally, but most importantly, I would like to pay my deepest gratitude to my family members for their love and encouraging. Words from them are always gentle, but always as heavy as gold pushing me step forward.

# Table of Contents

# List of Figures

viii

ix

# List of Tables

# Chapter 1. Introduction

## 1.1 Research area

Inconel 718 which is widely employed in the aerospace industry as Figure 1 presents, due to their high-temperature strength and high corrosion resistance. Due to the tough properties, the machining of Inconel 718 has more districts. As the finishing machining process, grinding is used as the last step for Inconel 718. As the research before, after the grinding process, tensile stress exists on the surface of the work piece which will reduce the life of component under stress corrosion or fatigue conditions and may result in unexpected failure. This thesis will focus on the control of the temperature distribution in the work piece which is the primary factor of the generating of the tensile stress. Induction heating will be employed as a controllable heating source.

**Figure 1 The application of Inconel 718**

## 1.2 Problem Statement

Compressive stresses are generally beneficial to fatigue life, creep life and resistance to stress corrosion cracking, whereas tensile residual stresses are usually detrimental to these same properties. The regular grinding process of Inconel 718 will generate tensile stress on the surface of parts that cannot be used as aerospace products because the potential fatigue failure [1]. A compressive superficial residual stress with a specific profile is mandatory to achieve certain fatigue tolerance according to the Federal Aviation Administration regulations [FAA, 2005]. For the special material properties, cutting force, tool wear, and

1

cutting temperature are characteristic features in the machining progress [2]. Machining process will employ compressive stress while thermal process will employ tensile one. The research [4] concludes thermal expansion and contraction in the grinding process was the most significant factor in the generation of tensile residual stresses [21]. A novel technology is figured out to solve the problem by creating a pre-grinding step to affect the temperature field before grinding. This thesis will focus on the controlling of the pre-grinding temperature with induction heating method combining cooling system. Simulation method is applied to demonstrate the effect of different induction parameters on the temperature distribution.

## 1.3 Objective

The objective of this thesis is to figure out an induction heating process to create a subsurface heating layer as the preparation of the grinding process. The processing includes induction heating system, concentrator system and cooling system. The effects of different parameters will be studied to embed the pre-grinding heating layer into work piece.

## 1.4 Impact

The generation of the subsurface heating layer changes the condition for the grinding process and the stress distribution. It will be a novel technology to improve the surface performance after grinding that is strictly required by the aerospace induction. The new technology shorten the grinding manufacturing progress by enhancing the superficial performance without short peening and other post processing method cutting cost and improving efficiency. With the novel technology, the nickel alloy parts can be produced with 100% superficial compressive stress without further heat treatment, cutting the cost a lot. The technology will benefit the U.S. manufacturing industry a high performance, low cost method to produce aerospace parts that trends to be done in developing countries because of the globalization competition. The high-tech manufacturing technology will bring the U.S. industry new opportunity of more working position and ability to compete in global market.

## 1.5 Expect results

In this thesis, a numerical model on the thermal aspect of the novel grinding process will be studied and realized with finite element analysis software COMSOL. The parameters will be investigated to provide a suggested recipe for novel technology that can be used for further stress analysis.

# Chapter 2.  Background

## 2.1  Residual stress control in super alloy processing

Inconel 718, a high strength, thermal resistant Nickel-based alloy presented in Table 1, has a wide range of applications in the aircraft industries, e.g. aircraft gas turbines, stack gas reheaters, reciprocating engines, etc. It maintains excellent mechanical properties and is corrosion resistant over a wide temperature range (-423°to 1300°F) [1]. The superficial stress of the aerospace parts is mandatory to achieve a certain fatigue life by Federal Aviation Administration regulations [FAA, 2005].

**Table 1 Physical constant of Inconel 718**

| | |
|---|---|
| Density, lb/in³ | |
| Annealed | 0.296 |
| Annealed and Aged | 0.297 |
| Melting Range, °F | 2300-2437 |
| °C | 1260-1336 |
| Specific Heat at 70°F, Btu/lb °F (at 21°C, J/kg °C) | 0.104 (435) |
| Curie Temperature, °F (°C) | |
| Annealed Material | <-320 (<-196) |
| Annealed and Aged Material | -170 (-112) |
| Permeability at 200 oersted and 70°F | |
| Annealed Material | 1.0013 |
| Annealed and Aged Material | 1.0011 |

Grinding is one of the most popular methods of machining hard materials widely used to produce surfaces of good dimensional accuracy and finish.[3] Because it is usually one of the final operations of the technological process, properties of surface layer created in grinding influence directly the functional properties of the work piece such as fatigue strength, abrasive and corrosion resistance, etc. On the other hand, Inconel 718 family is one of the most difficult to cut materials because they are very stain rate sensitive and readily work harden, and poor thermal conductivity, leading high cutting temperature at rake face [37]. Figure 2 presents the precision grinding for complex parts as a final machining step.

**Figure 2 Precision grinding process**

Low residual stress after grinding is an important requirement for surface integrity of stress sensitive components. If tensile residual stresses remain in the surface, the subsequent service life may be reduced under stress corrosion or fatigue conditions. [4] Compressive stresses are generally beneficial to fatigue life, creep life and resistance to stress corrosion cracking, whereas tensile residual stresses are usually detrimental to these same properties. In summary, residual stresses in machining are produced as a consequence of inhomogeneous plastic deformation induced by mechanical and thermal unit events associated with the process of chip formation (cutting) and the interaction between the tool nose region and the freshly machined work piece surface (squeezing). Plastic deformation due to forces parallel and perpendicular to the surface produces compressive residual stresses, whereas plastic deformation as a consequence of local heating shifts the balance towards tensile residual stresses. Phase transformations can support the development of both compressive and tensile residual stresses depending on the relative volume changes and the accompanying plastic deformations [4].
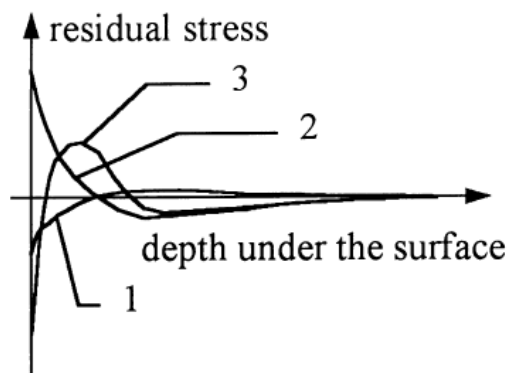


**Figure 3 Residual stress employed by grinding effects**

(a) Phase transformation; (b) Thermal expansion and contraction; (c) Plastic Deformation

4

Thermal expansion and contraction in the grinding process was the most significant factor in the generation of tensile residual stresses. Cutting temperatures generally increased with cutting speed and decreased with the increasing cooling efficiency of the cutting environment [31]. During grinding, high temperatures are generated at the interface between the wheel and the work piece as well as in the work sub-surface due to frictional heating and localized plastic deformation.[3]The problem of controlling stress is transformed into the problem of controlling grinding temperature. [4] Experience indicates that Tensile residual stresses are developed after the grinding temperature reaches a critical level at approximately 200°C which is hard to meet by regular coolant.

Various methods have so far been employed in order to improve fatigue strength, including optimization of geometric design, stronger materials and surface processing such as shot peening[17]. Shot peening has long been widely used as a low cost and simple method for increasing the fatigue strength of springs[24]. It is well known that shot peening a surface of a part or member creates a large compressive residual stress on the surface. It is also well known that this compressive residual stress contributes to the increased fatigue strength of the member. Shot peening can improve fatigue resistance by introducing a compressive residual stress in the surface layers of the material, making the nucleation and propagation of fatigue cracks more difficult [18]. However, shot peening cannot guarantee 100% compressive residual stress and may damage the well finished surface.

A novel grinding technology is to be developed to generate compressive superficial stress to meet both of the roughness and residual stress requirements.

## 2.2 Proposed technology

At the grinding zone, the thermal expansion of hotter material closer to the surface is partially constrained by the cooler subsurface material. This generates compressive thermal stresses near the surface which, if sufficiently big, cause plastic flow in compression. However during subsequent cooling, after the grinding heat passes, the plastically deformed material tends to reduce the volume in comparison to the beneath subsurface material, so the requirement of material continuity causes tensile stresses to develop near the surface.
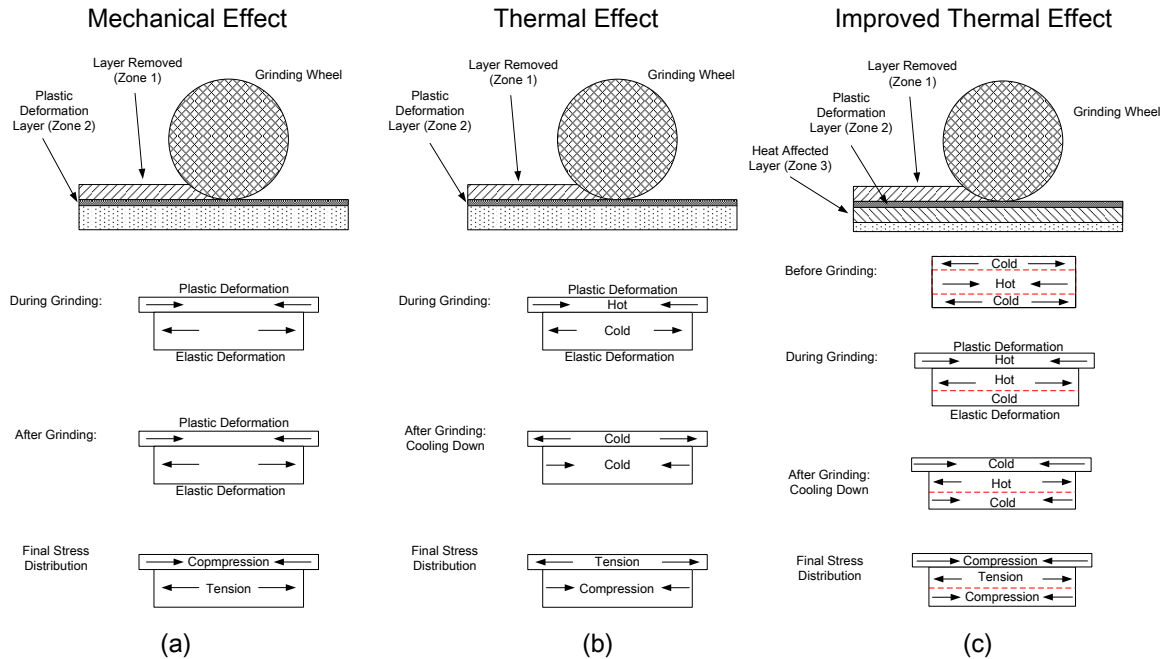
**Figure 4 The different ways how the grinding force and the grinding heat affect the residual stress**

(a) mechanical effect on the residual stress generation in the classic and proposed technology; (b) thermal effect on the residual stress generation in the traditional technology; and (c) thermal effect on the residual stress generation in the proposed technology.

In the technology, a 'hot' inner layer will be introduced in a controllable way before the grinding process occurs and the general mechanism of residual stress generation [Figure 4 (a) and Figure 4(b)] is changed during grinding process. As shown in Figure 4(c), the 'hot' layer exists before and during the grinding process. Before the grinding wheel engaging with the workpiece, the subsurface layer is pre-heated. This part of the work material experiences a higher temperature rise and intends to expand. During the grinding process, the superficial layer experiences a higher temperature than the subsurface layer, causing more severe plastic deformation and compressive stress than the subsurface layer. While after the grinding wheel pass the workpiece, the workpiece surface is subjected to rapid cooling. But the subsurface is also with a higher temperature. Both surface and subsurface material will be cooled simultaneously at similar rates, which maintain the superficial residual stress distribution to the final status.

## 2.3  Induction heating technology

### 2.3.1 The principle of induction

Induction heating has been used to heat electrically conductive materials since the early 1990's [14]. Induction heating is one of the most widely used methods for heat treatment of steel. It provides faster and more precise heating of local areas, consumes less energy and is considered environmentally friendlier than other methods [33]. Industrial applications of the technology include metal melting and heat treating, crystal growing, semiconductor wafer processing, high-speed sealing and packaging, and curing of organic coatings. The advantages of this technology include the

- Fast heating rate (6000°F/ s in foils)
- Instant start/stop (no warm up required for each cycle)
- Precise heat pattern (heating concentrated where needed)
- Noncontact heating (the heat applicator does not physically contact the part that is heated) [14]

An induction heating system usually consists of three distinct parts as Figure 5 presents: the power source (oscillator), an impedance matching circuit, and a load [14]. The load consists of a coil of wire (work coil) in close proximity to the heated material (work piece). Copper tubing is often used for the work coil in order to allow for water cooling during continuous operation, during normal operation, the oscillator supplies time varying current to the work coil, which produces an alternating magnetic field across the work piece. Since the work piece is electrically conductive, an eddy current is induced within it, and heat is generated from the resistance to the eddy current. Heat is also generated in magnetic materials from alternating magnetization and hysteresis.
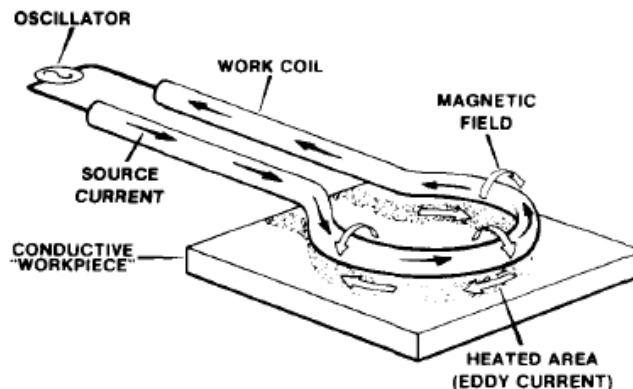


**Figure 5 Illustration of induction heating from induced eddy current**

With regard to the fact that material properties change drastically with temperature variations during an induction heating process and the difficulty in combining magnetic field and thermal analyses, analytical methods are very difficult to implement. Therefore, a computer-aided numerical tool, by using the finite-element method (FEM) is required to numerically model these coupled analyses, COMSOL Multiphysics is chosen in thesis [38].

### 2.3.2 The mathematical modeling of the electromagnetic field

The technique of calculating electromagnetic field depends on the ability to solve Maxwell's equations [25]. For general time-varying electromagnetic fields, Maxwell's equations in differential form can be written as:

Ampere's circuital law:

$$\nabla \times \vec{H} = \vec{J} + \frac{\partial \vec{D}}{\partial t} \qquad (1.1)$$

Faraday's law of induction:

$$\nabla \times \vec{E} = -\frac{\partial \vec{B}}{\partial t} \qquad (1.2)$$

Gauss's law for magnetism:

$$\nabla \cdot \vec{B} = 0 \qquad (1.3)$$

Gauss's law:

$$\nabla \cdot D = \rho \qquad (1.4)$$

where E is the electric field intensity, D is electric flux density, H is magnetic field intensity, B is the magnetic flux density, J is conduction current density and $\rho$ is the electric charge density.

Maxwell's equations not only have a purely mathematical meaning, they have a concrete physical interpretation as well. Equation 1.1 says that the curl of H has always two sources: conductive (J) and displacement $\rho$ currents. A magnetic field is produced whenever there are electric currents flowing in surrounding objects. From equation 1.2, one can conclude that a time rate of change in magnetic flux density B always produces the curling E field and induces currents in the surrounding area and therefore, in other words it produces an electric field in the area where such changes take place. The minus sign in

equation 1.2 determines the direction of that induced electric field. This fundamental result can be applied to any region in space.

The application of alternating voltage to the induction coil will result in the appearance of an alternating current in the coil circuit. According to Eq. (1.1), an alternating coil current will produce in its surrounding area an alternating magnetic field that will have same frequency as the source current. That magnetic field's strength depends on the current flowing in the induction coil, the coil geometry and the distance from the coil. The changing magnetic field induces eddy currents in the work piece and in other objects that are located near that coil. By Eq. (1.2), induced currents have the same frequency as the source coil current; however, their direction is opposite that of the coil current. This is determined by the minus sign in Eq. (1.2). According to Eq. (1.1), alternating eddy currents induced in the work piece produce their own magnetic fields, which have opposite directions to the direction of the main magnetic field of the coil. The total magnetic field of the induction coil is a result of the source magnetic field and induced magnetic fields.

As one would expect from analysis of Eq. (1.1), there can be undesirable heating of tools, fasteners, or other electrically conductive structures loaded near the induction coil.

In induction heating and heat treatment applications, an engineer should pay particular attention to such simple relations as (1.3) and (1.4). The short notation of Eq. (1.3) has real significance in induction heating and the heat treatment of electrically conductive body. To say the divergence of magnetic flux density is zero is equivalent to say that B lines have no source points at which they originate or end; in other words, B lines always form a continuous loop[25].

The above-described Maxwell's equations are in indefinite form because the number of equations is less than the number of unknowns. These equations become definite when the relations between the field quantities are specified. The following constitutive relations are additional and hold true for a linear isotropic medium.

$$D = \varepsilon \varepsilon_0 E \qquad (1.5)$$
$$B = \mu_r \mu_0 H \qquad (1.6)$$
$$J = \sigma E \qquad (1.7)$$

where the parameters $\varepsilon$, $\mu_r$ and $\sigma$ denote, respectively, the relative permittivity, relative magnetic permeability, and electrical conductivity of the material; $\sigma = 1/\rho$, where $\rho$ is electrical resistivity. $\varepsilon_0$ and $\mu_r$ are constants.

By taking Eq. 1.5 and 1.7 into account, Eq. 1 can be written as:

$$\nabla \times H = \sigma E + \frac{\partial(\varepsilon_0 \varepsilon E)}{\partial t} \qquad (1.8)$$

For most practical applications of the induction heating of metals, where the frequency of currents is less than 10MHz, the induced conduction current density J is much greater than the displacement current $\partial D / \partial t$, so the last term on the right hand side of Eq. (1.8) can be neglected. Therefore it becomes:

$$\nabla \times H = \sigma E \qquad (1.9)$$

After some vector algebra and using Eqs. (1.1), (1.2) and (1.6), it is possible to show that

$$\nabla \times \left( \frac{1}{\sigma} \nabla \times H \right) = -\mu_r \mu_0 \frac{\partial H}{\partial t} \qquad (1.10)$$

Since the magnetic flux density B satisfies a zero divergence condition as Eq. (1.3), it can be expressed in terms of a magnetic vector potential A as

$$B = \nabla \times A \qquad (1.11)$$

And then, from Eq. (1.2) and Eq. (1.11), it follows that

$$\nabla \times E = -\nabla \times \frac{\partial A}{\partial t} \qquad (1.12)$$

Therefore, after integration, one can obtain

$$E = -\frac{\partial A}{\partial t} - \nabla \varphi \qquad (1.13)$$

where $\varphi$ is the electric scalar potential. Eq. (1.7) can be written as

$$J = -\sigma \frac{\partial A}{\partial t} + J_s \qquad (1.14)$$

where $J_s = -\sigma \nabla \varphi$ is the source current density in the induction coil.

Taking the material properties as being piece wise continuous and neglecting the hysteresis and magnetic saturation it can be shown that

$$\frac{1}{\mu_0 \mu_r} (\nabla \times \nabla \times A) = J_s - \sigma \frac{\partial A}{\partial t} \qquad (1.15)$$

In induction heating problems, equation (1.15) can be solved assuming a sinusoidal time dependence of the magnetic vector potential A and magnetic permeability values corresponding to the first harmonic of the magnetic field intensity. With these assumptions the nonlinear electromagnetic equation can be solved iteratively till the convergence to steady magnetic permeability values is reached [35].

### 2.3.3 The mathematical modeling of the thermal process

In general, the transient (time-dependent) heat transfer process in a metal workpiece can be described by the Fourier equation:

$$c\gamma \frac{\partial T}{\partial t} + \nabla \cdot (-k\nabla T) = Q \qquad (1.16)$$

where T is temperature, $\gamma$ is the density of metal, c is the specific heat, k is the thermal conductivity of the metal, and Q is the heat source density induced by eddy currents per unit time in a unit volume. This heat source density is obtained by solving the electromagnetic problem.

Eq. (1.16) with suitable boundary and initial conditions, represents the three-dimensional temperature distribution at any time and at any point in the work piece. The initial temperature condition refers to the temperature profile within the workpiece at time t=0; therefore that condition is required only when dealing with a transient heat transfer problem where the temperature is a function not only of the space coordinates but also of time. The initial temperature distribution is usually uniform and corresponds to the ambient temperature. In some cases, the initial temperature distribution is nonuniform due to the residual heat after the previous technological process.

For most engineering induction heating problems, boundary conditions combine the heat losses due to convection and radiation. In this case the boundary condition can be expressed as:

$$-k\frac{\partial T}{\partial n} = \alpha(T_s - T_a) + C_s\left(T_s{}^4 - T_a{}^4\right) + Q_s \qquad (1.17)$$

where $\partial T/\partial n$ is the temperature gradient in a direction normal to the surface at point under consideration, $\alpha$ is the convection surface heat transfer coefficient, $C_s$ is the radiation heat loss coefficient, $Q_s$ is the surface loss and n denotes the normal to the boundary surface.

The Eq. (1.16) can be shown in Cartesian coordinates as:

$$c\gamma \frac{\partial T}{\partial t} = \frac{\partial T}{\partial X}\left(k\frac{\partial T}{\partial X}\right) + \frac{\partial}{\partial Y}\left(k\frac{\partial T}{\partial Y}\right) + \frac{\partial}{\partial Z}\left(k\frac{\partial T}{\partial Z}\right) + Q \quad (1.18)$$

This equation with boundary condition Eq. (1.17) are most popular equations for mathematical modeling of the heat transfer process in induction heating and heat treatment applications.

## 2.4 The design of coil and concentrator

### 2.4.1 Coil design

During induction heating, the relationship between time and temperature must be controlled exactly to obtain a uniform temperature distribution over the workpiece to control the formation of the subsurface heating layer. The coil design is very important to control the temperature accurately.

To design the coil for heating, there are several conditions should be kept in mind. The coil should be coupled to the part as closely as feasible for maximum energy transfer. It is desirable that the largest possible number of magnetic flux lines intersect the workpiece at the area to be heated. The denser the flux at this point, the higher will be the current generated in the part. The greatest number of flux lines in a solenoid coil is toward the center of the coil. The flux lines are concentrated inside the coil, providing the maximum heating rate there. Because the flux is most concentrated close to the coil turns themselves and decreases farther from them, the geometric center of the coil is a weak flux path. This effect is more pronounced in high-frequency induction heating. At the point where the leads and coil join, the magnetic field is weaker; therefore, the magnetic center of the inductor is not necessarily the geometric center. Due to the impracticability of always centering the part in the work coil, the part should be offset slightly toward this area [15].

In addition, the part should be rotated, if practical, to provide uniform exposure. The coil must be designed to prevent cancellation of the magnetic field. Putting a loop in the inductor (coil at center) will provide some inductance. The coil will then heat a conducting material inserted in the opening. The design at the right provides added inductance and is more representative of good coil design [15].

**Table 2 The coupling coefficient at different frequency**

| Coupling efficiency at frequency of: | 10 Hz | | 450 kHz | |
|---|---|---|---|---|
| Type of coil | Magnetic steel | Other metals | Magnetic steel | Other metals |
| Helical around workpiece ........ | 0.75 | 0.50 | 0.80 | 0.60 |
| Pancake ..................... | 0.35 | 0.25 | 0.50 | 0.30 |
| Hairpin ..................... | 0.45 | 0.30 | 0.60 | 0.40 |
| One turn around workpiece ...... | 0.60 | 0.40 | 0.70 | 0.50 |
| Channel ..................... | 0.65 | 0.45 | 0.70 | 0.50 |
| Internal ..................... | 0.40 | 0.20 | 0.50 | 0.25 |

Because of the above principles, some coils can transfer power more readily to a load because of their ability to concentrate magnetic flux in the area to be heated. Coupling efficiency is showed in Table 2 which is the fraction of energy delivered to the coil which is transferred to the workpiece.

There are kinds of coil designed as Figure 6 presents for different industry application, even for complex parts [15].
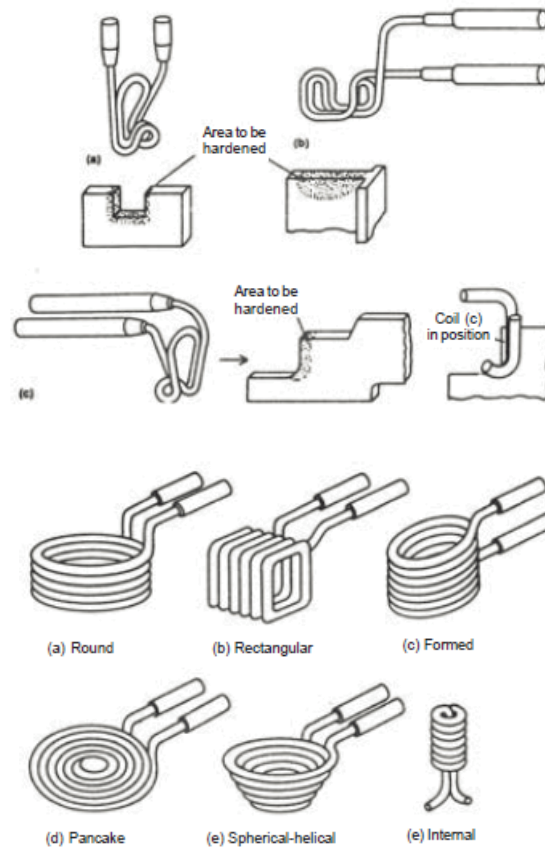


**Figure 6 The typical coil design for different application**

### 2.4.2 Concentrator design

Flux concentrators are magnetic materials which are utilized to gather the flux field set up during induction heating and thus to modify the resultant heating pattern.

Materials for flux concentrators are of two basic types: (1) packages of laminated silicon steel punchings used at frequencies below 10k Hz and (2) ferrites or powdered iron combinations for higher frequencies, including those in the radio-frequency range.

Flux concentrators, whether laminations or ferrites should be located directly in or on the coil. For example, placement in the center of a pancake coil collapses the over-all field to provide a higher density at the coil surface. In the same manner, insertion of a concentrator in a helical coil collapses the end flux outside the coil center. Physical characteristic of the concentrators are presented in Table 3.

**Table 3 Physical characteristic chart from Fluxtrol**

| Physical Characteristics Chart | | | | | | | |
|---|---|---|---|---|---|---|---|
| | | Primary Products | | | | Specialized Products | |
| Properties | Units | Fluxtrol A | Fluxtrol 50 | Ferrotron 559H | | Fluxtrol 25 | Ferrotron 119 |
| Product Identification Color | | Green | Yellow | Grey | | Red | Black |
| Density ± 2% | g/cm3 | 6.6 | 6.1 | 5.9 | | 5.5 | 4.8 |
| Operating Frequency Range | kHz | 1–50 | 10–1000 | 10–3000 | | 10–3000 | 10–5000 |
| Major Frequency Area | kHz | 3–30 | 50–500 | 50–1000 | | 50–500 | 100–1000 |
| Initial Permeability | None | 63 | 36 | 16 | | 23 | 7 |
| Maximum Permeability | None | 120 | 55 | 18 | | 28 | 8 |
| Saturation Flux Density | Tesla | 1.6 | 1.5 | 1.0 | | 1.3 | 0.8 |
| Temperature Resistance | Centigrade | 250 Long Term 300 Short Term | 250 Long Term 300 Short Term | 250 Long Term 300 Short Term | | 250 Long Term 300 Short Term | 250 Long Term 300 Short Term |
| Resistivity | kOhmcm | 0.5 | 0.5 | >15 | | >100 | >100 |

# Chapter 3. The modeling and simulation of the novel technology

## 3.1 Simulation process design

### 3.1.1 The simulation software

Induction heating computer simulation has gained wider acceptance due to significant improvements in both computer hardware and software. More and more companies are beginning to use computer simulation for practical induction process and system design [36]. To simulate the process of induction heating, we apply finite element analysis software tool to calculate the parameters subjecting to a comprehensive study. This simulation is based on the software of COMSOL which is widely used in the application of Multiphysics modeling. The modules of AC/DC, structural mechanics and heat transfer are used as Figure 7.
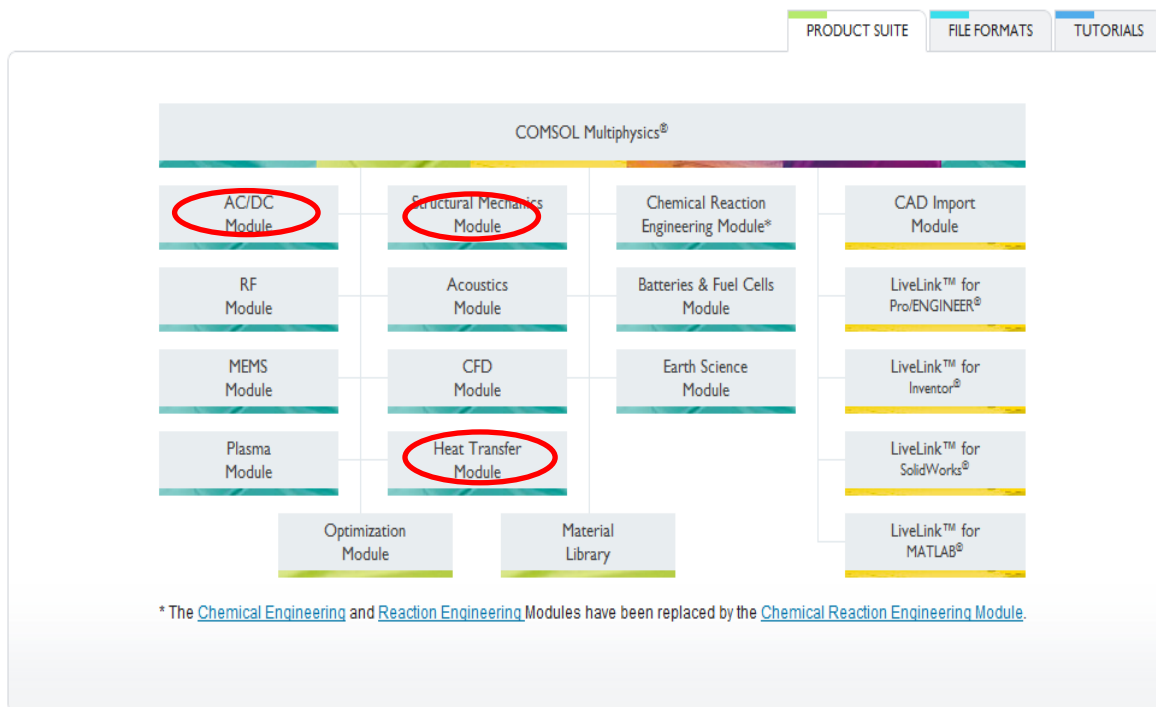


**Figure 7 The COMSOL Multiphysics software**

### 3.1.2 The simulation process

The simulation contains two primary parts, induction and heat transfer. The induction process that is determined by the coil and the concentrator parameters including current and frequency input, the heat transfer process has three heat sources at different period of time, including the heat generated by the

15

induction process, the cooling system, and the grinding heat. Speed represents the motion of the work piece during the whole process presented in Figure 8.
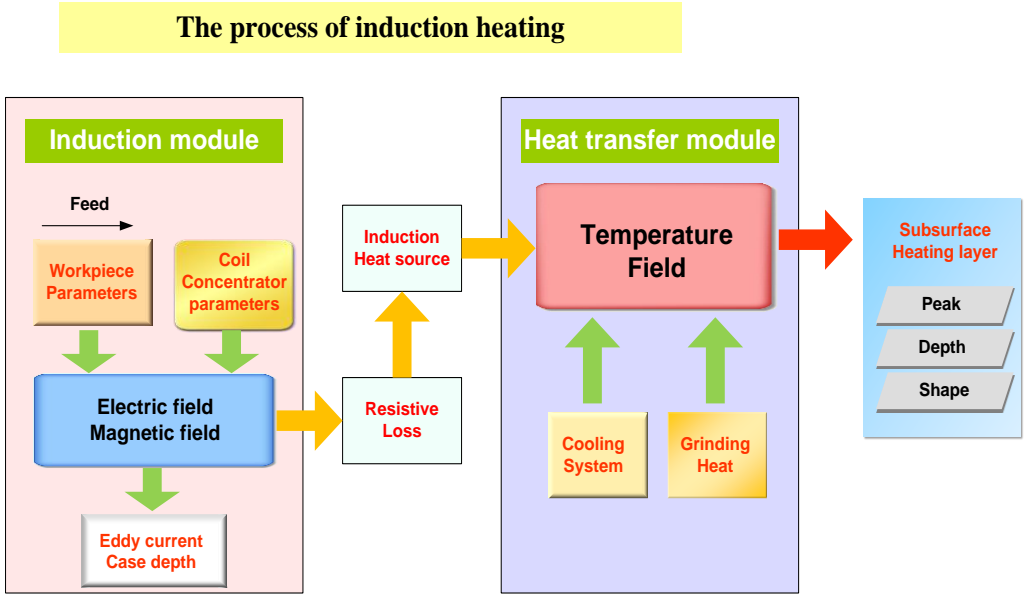


**Figure 8 The process of induction heating**

### 3.1.3 The timing plan for induction process

To reach the final objective, generating a proper value, depth and shaped subsurface heat layer, time interval should be considered as an important input parameters as showed in Figure 9. After 5s, the input is gone with only regular convection cooling with air existing.
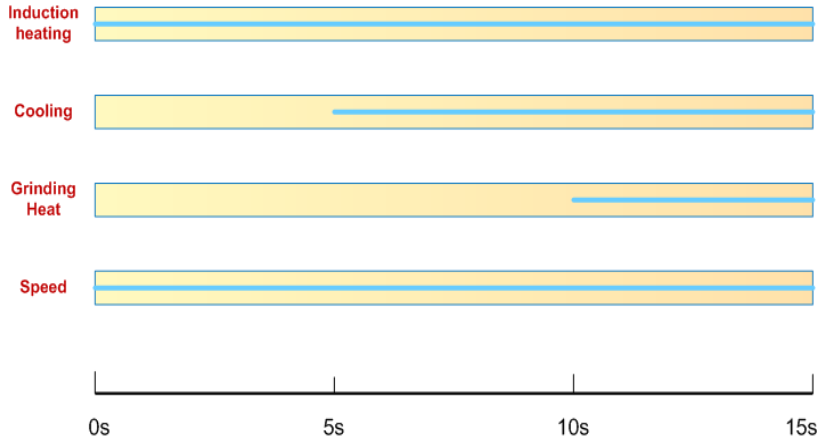


**Figure 9 The default time chart for induction heating process**

16

### 3.1.4 The flow chart for the induction process

The flow chart Figure 10 for the study is showed in the figure to describe the process clearly step by step. The chart also describes the parameters for each process that can be studied independently to some extent. Yellow areas show the study that has finished and green areas represent the study in future. The first input variations are current and frequency that determine the energy too applied on the coil. Coil shape and material combining concentrator parameters will affect the electromagnetic field based on the Maxwell's equations that can be obtained when the boundary condition is provided. With the eddy current calculated from Maxwell's equations, the resistive loss can be obtained as heating resource. The heat transfer module will present the temperature field generated by current input. To finally get the subsurface heating layer, the cooling system will help to form the temperature field by control the cooling time and position. Further study will focus on the stress distribution.



**Figure 10 The flow chart of induction heating**

17

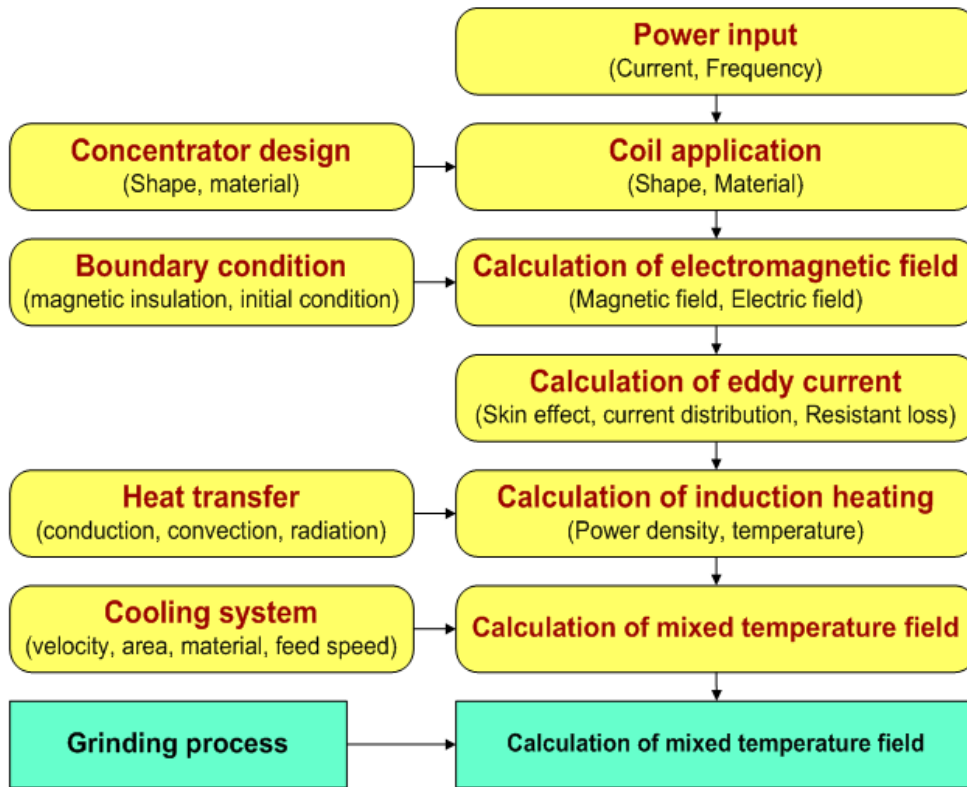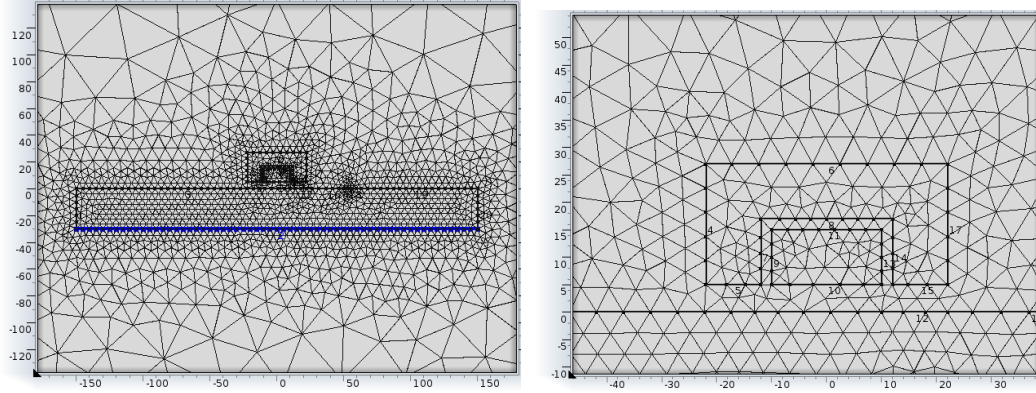### 3.2  The simulation conditions

#### 3.2.1 The geometry model design

To study the induction process, a 2D model is built as showed in Figure 11. 2D model is preferred to have a better efficiency with the computer and the thickness is set to 100 mm. In the figure, A is the coil set to the material of copper with concentrator outside that has special electric parameters, B is the workpiece made of Inconel 718 that is prepared to grind marked with E, C represents the cooling system that has convection heat transfer coefficient on it, D is the grinding contacting area with a width of 2mm, and F is the air that plays a role in the propagation of electromagnetic field. The space around the elements is assigned air parameters with a shape of circle of which center is the same with the coil center to keep the electromagnetic lines closed.During the analysis, the position relationship for the elements in Figure 11 is also studied, such as the gap between coil and workpiece, the gap between the coil and concentrator. Cooling position is also studied.



**Figure 11 The geometry model**

Unit: mm, A: Coil, B: Workpiece, C:Cooling agent, D:Grinding heat flux, E: Concentrator

The meshing function provide by COMSOL is presented in Figure 12 in which the air area is meshed with a large scale while the coil and workpiece is meshed with smaller elements that can be implemented separated.

**Figure 12 The meshing provided by COMSOL**

The temperature profile inside the items depends on geometry configurations, the coupling of the samples and material properties[32]. In this thesis we analyze the temperature inside the workpiece by varying parameters, the current inside the coils, to obtain the subsurface heating layer.

### 3.2.2 The materials parameters

#### a) Coil parameters

Coil parameters are presented in Table 4. Coil and concentrator system should have its own cooling system, so the thermal parameters are not considered in the simulation process. It was assumed that the specimen structures were homogenized at 6003C and initially free of residual stresses [20]. The material selected is brass. The temperature dependence of the magnetic permeability is usually neglected so that the magnetic permeability and electric permittivity are assigned to 1 [26].

**Table 4 Parameters of coil**

|  | Parameters | Sign | Value | Unit |
|---|---|---|---|---|
| 1 | Magnetic permeability | $\mu$ | 1 | H/m |
| 2 | Electric permittivity | $\varepsilon$ | 1 | F/m |
| 3 | Electric conductivity | $\sigma$ | 5.95e7 | S/m |
| 4 | Current | J | 400 | A |
| 5 | Current density | Js0 | 20000 | A/m |
| 6 | Frequency | f | 100k | Hz |

**b) Cooling condition**

Water is selected as the cooling agent and the boiling water can have a high heat transfer efficient. The convection heat transfer coefficient is dependent on the type of media, gas or liquid, the flow properties such as velocity, viscosity and other flow and temperature dependent properties. Table 5 presents the value of HTC will be between 5,000 and 50,000. For water, the value can be as high as 10,000 $W/m^2K$.

**Table 5 Parameters for cooling system**

| | Parameters | Sign | Value | Unit |
|---|---|---|---|---|
| 1 | heat transfer efficient | $h$ | 5,000-50,000 | $W/m^2K$ |

**c) Concentrator**

Concentrator has the same material with the coil but the permeability as Table 6 presents. Usually the concentrator material is preferred to have a smaller electric conductivity and larger magnetic permeability so that the resistive loss of the concentrator can be limited and can concentrate the electromagnetic field to control the heating process more precise.

**Table 6 Parameters of concentrator**

| | Parameters | Sign | Value | Unit |
|---|---|---|---|---|
| 1 | Magnetic permeability | $\mu$ | 20-100 | H/m |
| 2 | Electric permittivity | $\varepsilon$ | 1 | F/m |
| 3 | Electric conductivity | $\sigma$ | 5.95e7 | S/m |

**d) Atmosphere**

The air atmosphere affects the distribution of the magnetic field the parameters are set as Table 7 presents.

**Table 7 Parameters of the atmosphere**

| | Parameters | Sign | Value | Unit |
|---|---|---|---|---|
| 1 | Magnetic permeability | $\mu$ | 1 | H/m |
| 2 | Electric permittivity | $\varepsilon$ | 1 | F/m |
| 3 | Electric conductivity | $\sigma$ | 0 | S/m |

### 3.2.3 The properties of Inconel 718

#### a) Introduction of Inconel 718

Inconel 718 [13] (UNS N07718/W. Nr. 2.4668) is a high-strength, corrosion-resistant nickel chromium material used at -423° to 1300°F. The age-harden able alloy can be readily fabricated, even into complex parts. Its welding characteristics, especially its resistance to post weld cracking, are outstanding. Examples of these are components for liquid fueled rockets, rings, casings and various formed sheet metal parts for aircraft and land-based gas turbine engines, and cryogenic tankage. It is also used for fasteners and other instrumentation parts. Chemical composition and physics properties of Inconel 718 are listed in Table 8.

**Table 8 Chemical composition of Inconel 718**

| | |
|---|---|
| Nickel (plus Cobalt) | 50.00-55.00 |
| Chromium | 17.00-21.00 |
| Iron | Balance* |
| Niobium (plus Tantalum) | 4.75-5.50 |
| Molybdenum | 2.80-3.30 |
| Titanium | 0.65-1.15 |
| Aluminum | 0.20-0.80 |
| Cobalt | 1.00 max. |
| Carbon | 0.08 max. |
| Manganese | 0.35 max. |
| Silicon | 0.35 max. |
| Phosphorus | 0.015 max. |
| Sulfur | 0.015 max. |
| Boron | 0.006 max. |
| Copper | 0.30 max. |

| | |
|---|---|
| Density, lb/in³ | |
| Annealed | 0.296 |
| Annealed and Aged | 0.297 |
| Melting Range, °F | 2300-2437 |
| °C | 1260-1336 |
| Specific Heat at 70°F, Btu/lb °F (at 21°C, J/kg °C) | 0.104 (435) |
| Curie Temperature, °F (°C) | |
| Annealed Material | <-320 (<-196) |
| Annealed and Aged Material | -170 (-112) |
| Permeability at 200 oersted and 70°F | |
| Annealed Material | 1.0013 |
| Annealed and Aged Material | 1.0011 |

### b) The electromagnetic properties of Inconel 718

The properties of the Inconel 718 alloy are listed in Table 9, in which the temperature coefficient is used for the calculation of the electric conductivity because it is temperature dependent.

**Table 9 Parameters of the electromagnetic properties of Inconel 718**

|   | parameters | sign | Value | Unit |
|---|---|---|---|---|
| 1 | Magnetic permeability | $\mu$ | 1 | H/m |
| 2 | Electric permittivity | $\varepsilon$ | 1 | F/m |
| 3 | Electric resistive | $r$ | 1.754E-8 | $ohm \cdot m$ |
| 4 | Temperature coefficient | alpha | 0.0039 | $K^{-1}$ |

The electric conductivity is varied by the temperature. $\sigma=1/(r0*(1+alpha*(T-T0)))$ as Figure 13
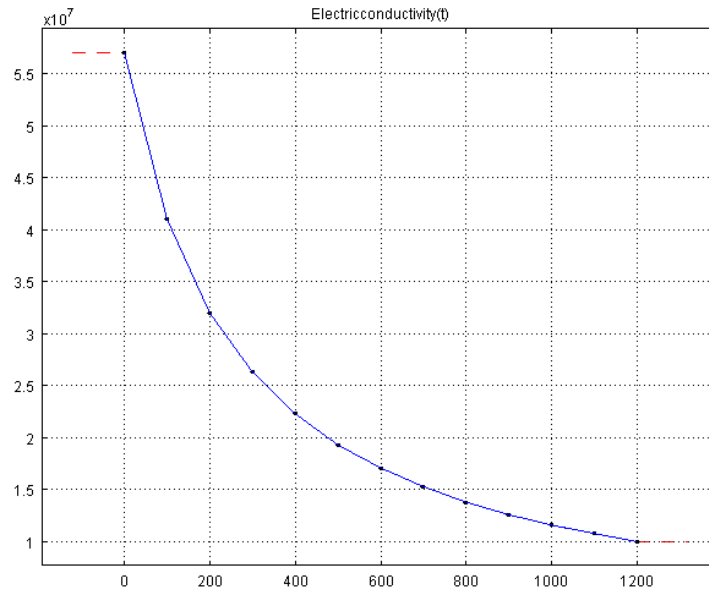


**Figure 13 Electric conductivity**

(Unit S/m)

22

### c) The heat transfer properties of Inconel 718

Thermal parameters are function of the temperature. During the process the heat capacity and thermal conductivity are considered as Figure 14 and Figure 15.
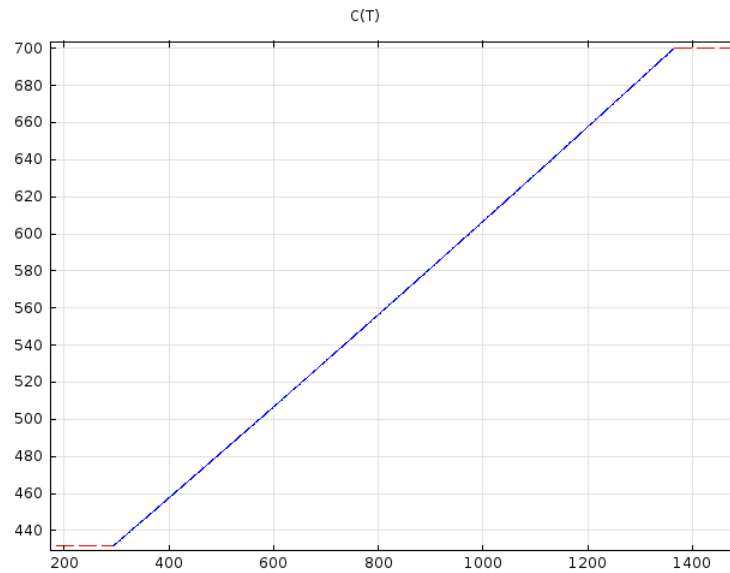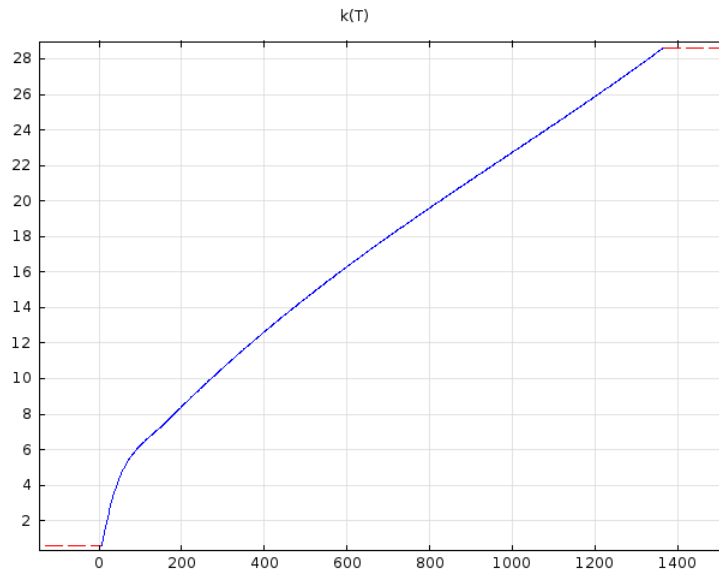


**Figure 14 Heat capacity**

(Unit: J/(kg*K))



**Figure 15 Thermal conductivity**

(Unit: W/(w*K))

23

### 3.2.4 Grinding heat

Simplified as a heat flux as wide as 2mm and with a heat flux value input, it will contribute to the final temperature field distribution. The right-angled triangle model is selected presented in The strength of the heat source in a theoretical modeling should vary in the grinding zone and could be properly described by a triangular profile with an adjustable apex to accommodate the effect of different grinding operations. Inside a grinding zone there is usually much less coolant, and the coolant there may evaporate. Thus the convection rate inside is generally lower [23]. In our model the heat flux is defined as Figure 16, a right-angle triangle with a width of 2mm which is the contact area between grinding wheel and work piece.

The strength of the heat source in a theoretical modeling should vary in the grinding zone and could be properly described by a triangular profile with an adjustable apex to accommodate the effect of different grinding operations. Inside a grinding zone there is usually much less coolant, and the coolant there may evaporate. Thus the convection rate inside is generally lower [23]. In our model the heat flux is defined as Figure 16, a right-angle triangle with a width of 2mm which is the contact area between grinding wheel and work piece. and the traditional heat flux will be around 1e7 as Table 10 presents [22].

**Table 10 parameters for grinding heat**

|   | Parameters | Sign | Value | Unit |
|---|------------|------|-------|------|
| 1 | Heat flux  | $q$  | 1e7   | W/m$^2$ |

The strength of the heat source in a theoretical modeling should vary in the grinding zone and could be properly described by a triangular profile with an adjustable apex to accommodate the effect of different grinding operations. Inside a grinding zone there is usually much less coolant, and the coolant there may evaporate. Thus the convection rate inside is generally lower [23]. In our model the heat flux is defined as Figure 16, a right-angle triangle with a width of 2mm which is the contact area between grinding wheel and work piece.

## 3.3  The operation parameters

The parameters that will be studied in the project are presented in Table 11 including the current input, coil and concentrator properties and cooling system.

**Table 11 The parameters to study**

|  | **Induction Module** | **Parameter to study** | **Output parameters** |
|---|---|---|---|
| 1 | Current input | Current | Electric field |
| 2 |  | Frequency | Magnetic field |
| 3 | Coil properties | Relative permeability | Case depth |
| 4 |  | Electric conductivity | Resistive loss |
| 5 |  | Relative permittivity |  |
| 6 |  | Dimension |  |
| 7 |  | Shape |  |
| 8 |  | Distance from workpiece |  |
| 9 | Concentrator | Relative permeability |  |
| 10 | properties | Electric conductivity |  |
| 11 |  | Relative permittivity |  |
| 12 |  | Dimension |  |
| 13 |  | Shape |  |
| 14 |  | Gap between the concentrator and coil |  |
| 15 | Cooling system | Feed speed | Temperature distribution |
| 16 |  | Cooling position | The highest temperature |
| 17 |  | Cooling time | The depth of the peak |
| 18 |  | Cooling agent heat transfer coefficient | Shape of heat layer |

# Chapter 4.  Simulation result

The simulation of induction process can be divided into three steps, the electromagnetic process, the heat transfer process and heat transfer combining the cooling system.

Each process can be studied independently.  The requirement for induction is to generate a certain value of resistive loss, which will be the main heat resource input of the heat transfer process. Based on the resistive loss value, we can simulate the induction process by adjusting the parameters of the coil

parameters and concentrators, besides the distance and shape information. On the other hand, the input of current and frequency can be studied at the same time.

The resistive loss will heat the workpiece to a certain temperature. Based on the TTT diagram of Inconel showed in Figure 16, the highest temperature should not exceed 886 ℃, because upon that phase transfer may happen. With this heat resource input, we can have a comprehensive study on the cooling system and the process of induction, including the time interval between heating and cooling to have a proper subsurface heat layer. 800℃ is selected in the simulation process.

Computer modeling provides the ability to predict how different factors may influence the transitional and final heat treating conditions of the workpiece and what must be accomplished in the design of the induction heating system to improve the effectiveness of the process and guarantee the desired heating results. Computer model is showed in the literature review part and the model is applied in the software of COMSOL.
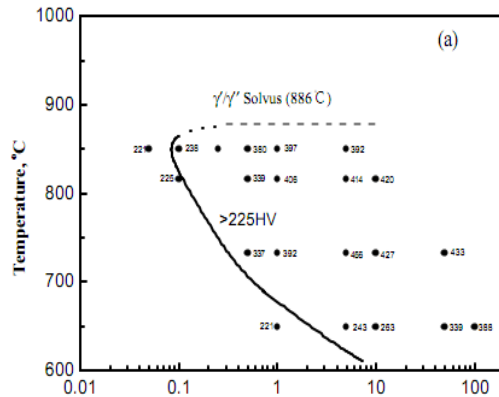


**Figure 16 The hardness temperature diagram for Inconel 718**

## 4.1 The electromagnetic phenomenon simulation

In this section, the induction process is simulated to present the electromagnetic phenomenon. The Figure 17 presents the distribution of the electromagnetic field and Figure 18 presents the induction heating effects. Several electromagnetic phenomena are also simulated including the skin effect, the slot effect and the proximity effect. Eddy current will be induced inside the work piece, and becomes the heat sources of the induction heating process. The alternating current in the inductor is not uniform, either does the eddy current distribute in the work piece.
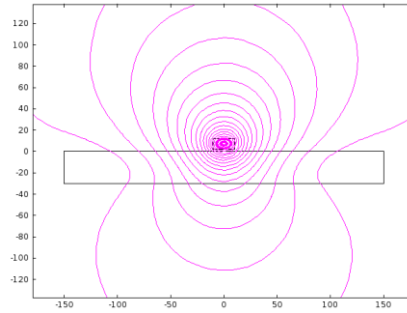
**Figure 17 The distribution of the electromagnetic field**

The effectiveness of the heating is related to the following items: 1) shape of the plate surface subjected to the variable magnetic flux; 2) area of the region exposed to the magnetic flux; 3) position of the region exposed to the magnetic flux with respect to the plate center[34].

In high-frequency induction heating, the induced current is usually not uniform throughout the workpiece [38]. This heat sources nonuniformity causes a nonuniform temperature profile in the workpiece as Figure 18 presents. To obtain a high efficient heating effect, parameters should be well investigated. In this part, the phenomenon is studied.
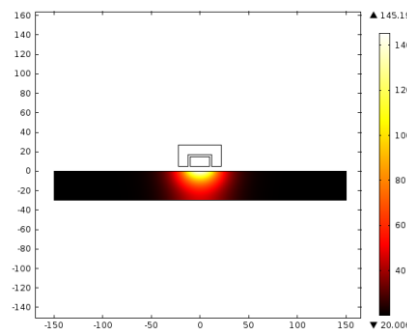


**Figure 18 The temperature field with by induction heating process**

### 4.1.1 Skin effect

When a direct current flows through a conductor that stands alone, the current distribution within the conductor's cross-section is uniform. However, when an alternating current flows through the same conductor, the current distribution is not uniform. The maximum value of the current density will always be located on the surface of the conductor and the current density will decrease from the surface of the conductor toward its center. This phenomenon of nonuniform current distribution within the conductor cross-section is called the skin effect, which always occurs when there is an alternating current. Therefore

27

the skin effect will also be found in a workpiece located inside an induction coil. This is one of the major factors that cause concentration of eddy current in the surface layer of the workpiece.

The skin depth is defined as the depth below the surface of the conductor at which the current density has fallen to 1/e (about 0.37) of JS. In normal cases it is well approximated as:

$$\delta = \sqrt{\frac{2\rho}{\omega\mu}}.$$

Where    $\rho$ = resistivity of the conductor

$\omega$ = angular frequency of current = $2\pi$ × frequency

$\mu$ = absolute magnetic permeability of the conductor
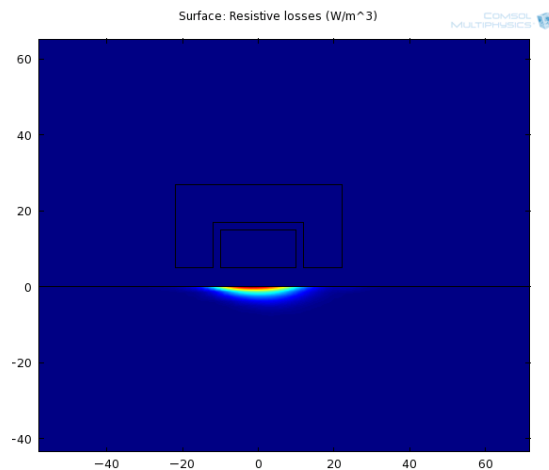


**Figure 19 The skin effect**

Based on the equation, the value of penetration depth varies with the square root of electrical resistivity and inversely with the square root of frequency and relative magnetic permeability. From the simulation result seen in Figure 19, current concentrates near the very surface, larger frequency value will benefit on the skin depth.

The skin effect is of great practical importance in electrical applications using alternative current. Because of the effect, approximately 86% of the power will be concentrated in the surface layer of the conductor. This layer is called the reference depth $\delta$. The degree of skin effect depends on the frequency and material properties of the conductor. There will be a pronounced skin effect when high frequency is applied or when the radius of the workpiece is relatively large.

### 4.1.2 The distribution of AC in coil

The current distributed in the coil is not symmetrical but on the surface of coil due to the skin effect. The induction process is sensitive with the distance between the coil and the workpiece, so the distribution of the alternating current should be paied enough attention.
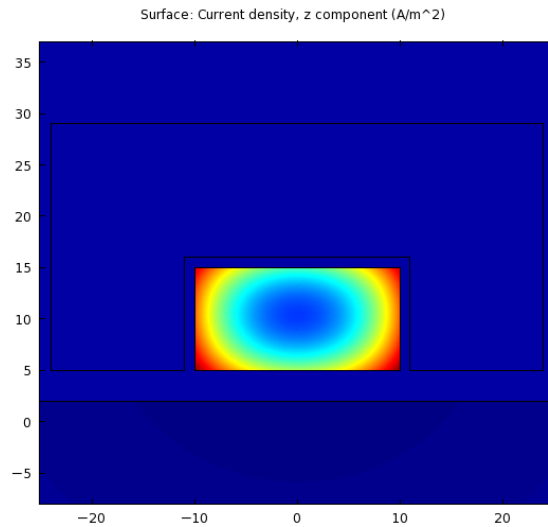


**Figure 20 The distribution of the alterlating current inside the coil**

**The frequency is as low as 50Hz**

The Figure 20 presents the alternating current distribution under the frequency of 50Hz which is relatively low in the induction heating technology. The depth of the current could be calculated with same way of skin depth. The Figure 21 presents the distribution of the current at a high frequency of 50k Hz in which current almost becomes face current on the surface of the coil.

### 4.1.3 The proximity effect

The current of inside the coil will distribute close to the side of the workpiece surface due to the proximity effect. When the current carrying conductor is placed to the workpiece, the current distribution will concentrate in the areas facing each other when the direction of the current is different. Due to Faraday's law, eddy current induced within the workpiece have an opposite direction to that of the source current of conductor. Figure 21 presents the current concentrates on the side of the surface of work piece, the concentrator is disabled at this circumstance.

Surface: Current density, z component (A/m^2)
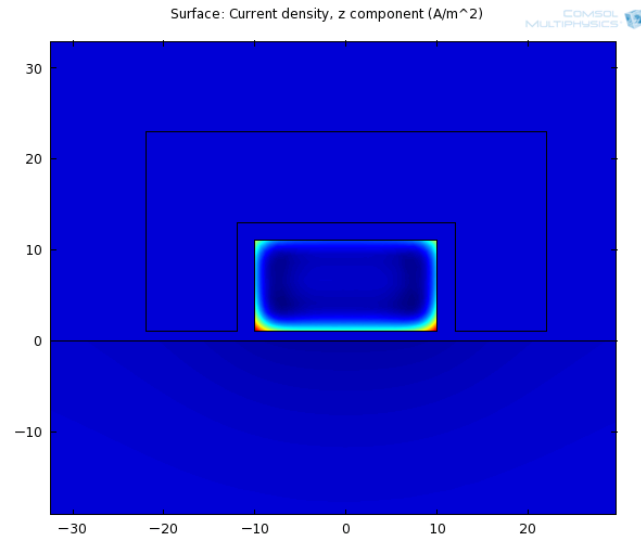
**Figure 21 The distribution of the current in the induction process**

### 4.1.4 The slot effect

The concentrator will affect the distribution of the current inside the coil simulated in Figure 22. As the proximity effect, all the current should concentrate to the side of workpiece. The magnetic concentrator will squeeze the current to the open surface of the concentrator, in other workds to the open area of slot. **Error! Reference source not found.**The actual current distribution in the conductor depends on the requency, magnetic field intensity, geometry, and electromagnetic properties of the conductor and the concentrator. Slot and proximity effects play a particularly important role in the proper design of coils for induction heating.



Surface: Current density, z component (A/m^2)
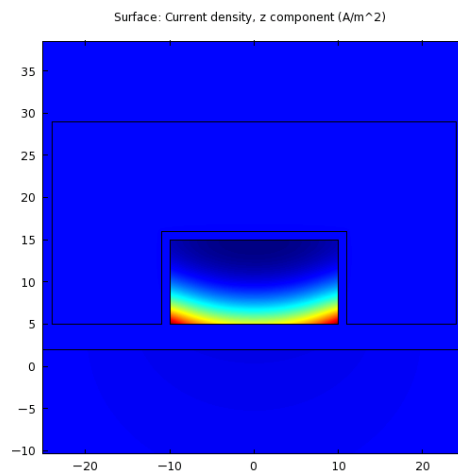
**Figure 22 The slot effect**

## 4.2  The electromagnetic analysis

### 4.2.1 The distribution of the magnetic field

The magnetic field is determined by the Maxwell's equations. Based on the equations, the magnetic field distribution is showed in Figure 23 and Figure 24 which indicate the magnetic field concentrates on the surface area of the workpiece. The concentration finally causes the skin effect because the alternating magnetic field generates the eddy current on the surface of the workpiece. Concentrator will benefit on changing the distribution of the magnetic field limiting it focusing more on the surface of workpiece.
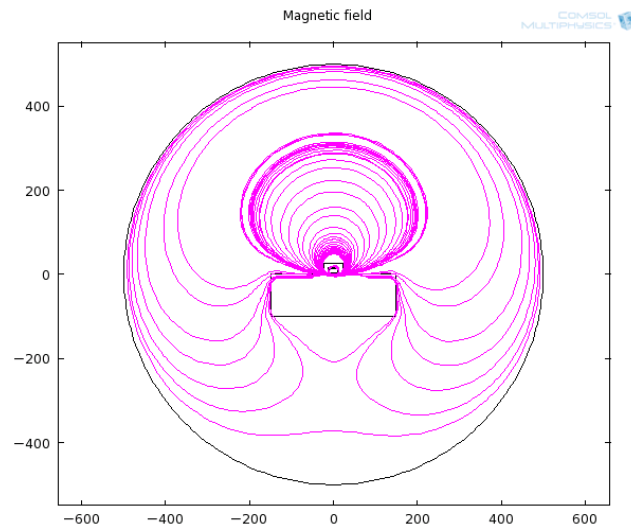


**Figure 23 The magnetic field lines**

From Figure 24, the magnetic field lines are concentrated near the surface of workpiece, the magnetic field will generate current and result in the skin effect. Most of the magnetic induction line will get through the surface of coil and the space between the coil and workpiece. The closer the coil to the workpiece, the more magnetic induction line will get through. So the gap is also an important parameter for induction heating process.

31
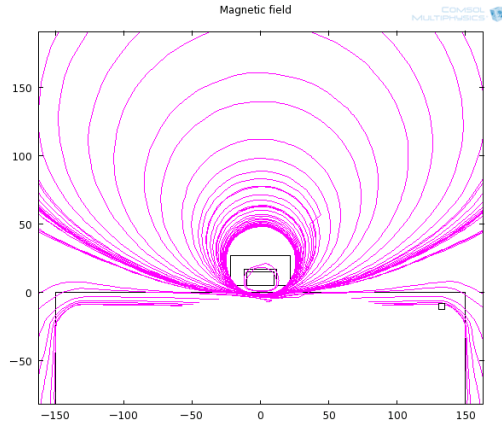
**Figure 24 The magnetic field lines near the surface of work piece**

### 4.2.2 The distribution of the current

The current exists near the surface of the workpiece as presented in Figure 25. As mentioned in 4.1, the skin effect eventually determines current will concentrate near surface as a heating source.
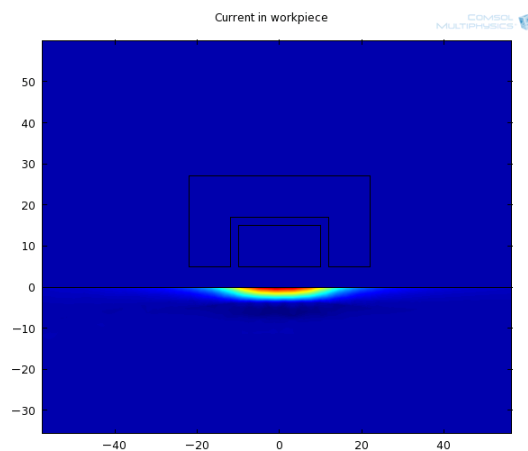


**Figure 25 The current distributes near the surface**

Eddy current is the heat sources for the induction heating process, the concentration of eddy current will determine the power input to a large extent. It helps to determine the current and frequency in the process.

### 4.2.3 The resistive loss

The resistive loss is the mainly energy for the heating process, it is calculated from the eddy current, so the distribution seems similar with the current. These currents produce heat by Joule effect ($I^2R$). So the resistive loss showed in Figure 26 is similar to the distribution of eddy current. The resistance of material

is specified by the Inconel 718 properties, so to control the energy input, the eddy current generation should be studied systematically.
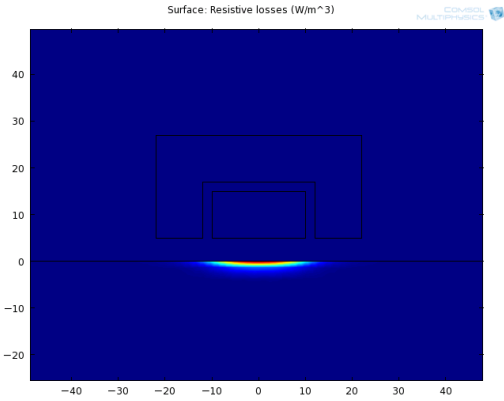


**Figure 26 The distribution of the resistive loss**

### 4.2.4 The effect of current on resistive loss

From the definition of skin effect, the current won't change the skin depth, but as the increasing of the current, the resistive loss increase significantly as Figure 27 presents. The increasing of the current input will also result in the increasing of the eddy current inside the workpiece. To improve the heating speed, improving the current input is an efficiency way, while the current needs to be controlled in certain value.
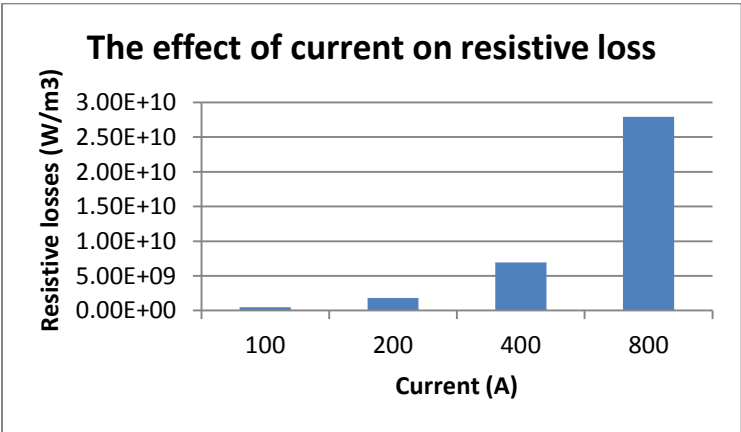


**Figure 27 The effect of current on resistive loss**

### 4.2.5 The effect of frequency on resistive loss and case depth

The frequency affects the resistive loss and determines the skin depth of workpiece as Figure 28 and Figure 29 presents. The larger frequency will increase the resistive loss. When the frequency increases

from 100kHz to 200kHz, the resistive loss is almost doubled. While when the frequency increases, the case depth decreases which means the heat source can be deeper and will benefit on the subsurface heating effect.
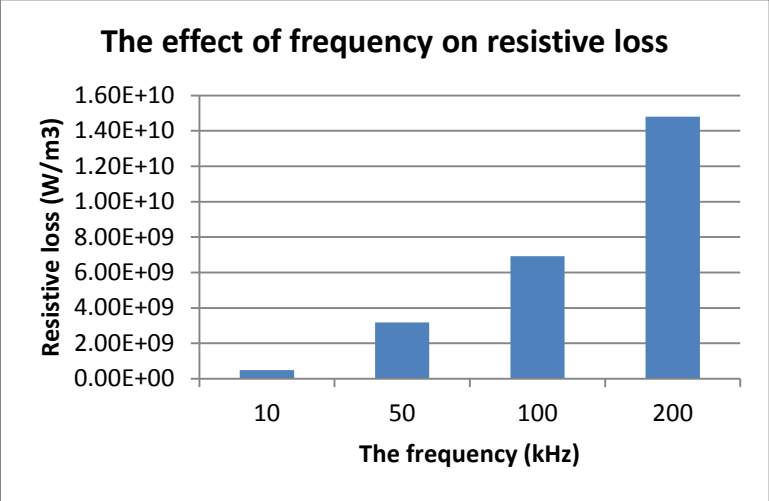


**Figure 28 The effect of frequency on resistive loss**

The skin depth can be as high as 5.5mm with a frequency value of 10k Hz. For induction heating process, the frequency is large most time to keep energy input.
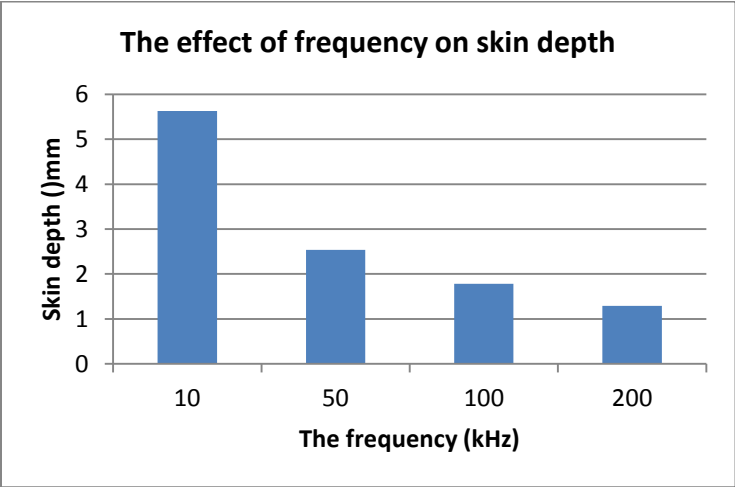


**Figure 29 The effect of frequency on skin depth**

### 4.2.6 The effect of the distance between coil and workpiece on resistive loss

The distance of coil from workpiece will affect the heating efficiency. It's obvious that the closer the coil to the workpiece, the stronger the electromagnetic field is. At the same time, the induction current will be larger in the workpiece as Figure 30presents.
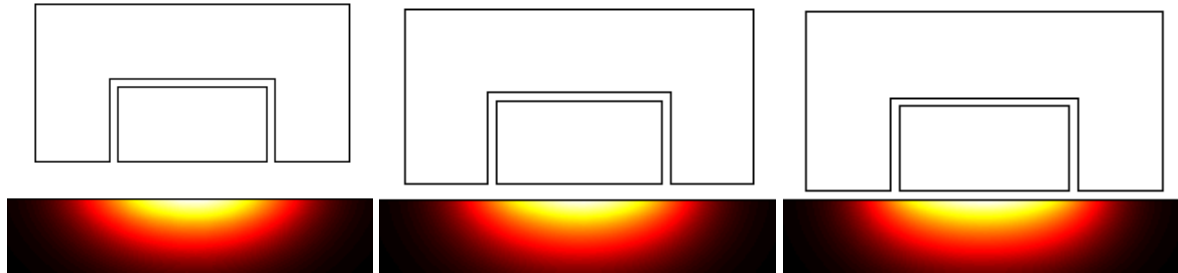


**Figure 30The effect gap between work piece and coil**

Resistive loss of the workpiece varies with the gap, smaller gap will concentrate the power input well and result in a better heating efficiency as Figure 31 presents.
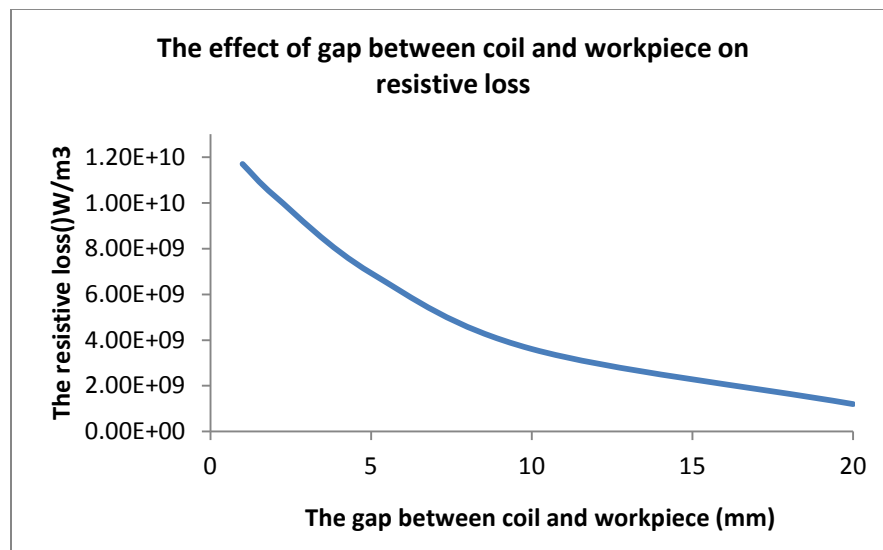


**Figure 31 The effect of gap between coil and workpiece on resistive loss**

### 4.2.7 The effects of concentrator on induction heating

Concentrator is used to improve the induction heating in industry that helps concentrate the electromagnetic lines forcing energy to a certain area to be heated. In Figure 32, the electromagnetic lines distribute relatively uniform around the work piece, closer to the workpiece, the density is larger. While in Figure 33, most of the electromagnetic lines gather inside the concentrator and the density of the lines that also reflect the intensity of the electromagnetic filed becomes large.
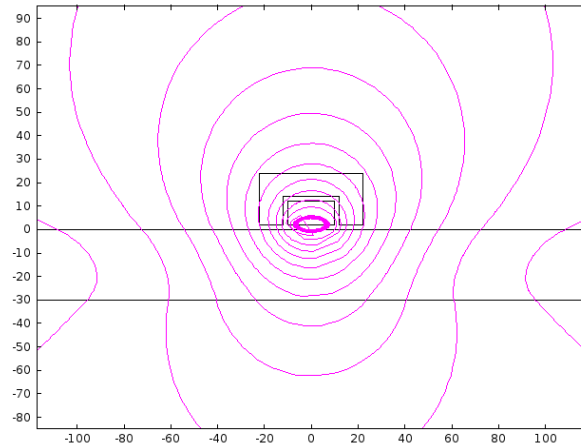


**Figure 32 Electromagnetic lines without concentrator**

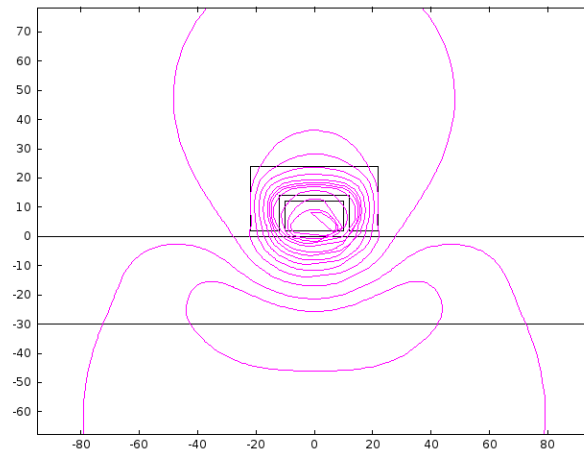Simulation results also indicate that in same condition, the temperature of the workpiece increases from 406℃ to 561℃



**Figure 33 Electromagnetic lines with concentrator**

## 4.3 The thermal analysis

The objective of the research is to generate a subsurface heating layer as a preparation for the grinding process. The induction heating will generate a temperature field inside the workpiece and the velocity field is demanded by the process. And to avoid unnecessary factors during the novel grinding process, the surface temperature should keep the same as usual at a relative low temperature. So the cooling system is applied to the system following the induction heating process.

### 4.3.1 The temperature distribution

The Figure 34 presents the coil begins to heat the workpiece by the eddy current generated by the alternating current. The very surface will form a high temperature area and heat transfer process occurs. Workpiece will be heated to 800℃ around first before combining cooling system and motion.
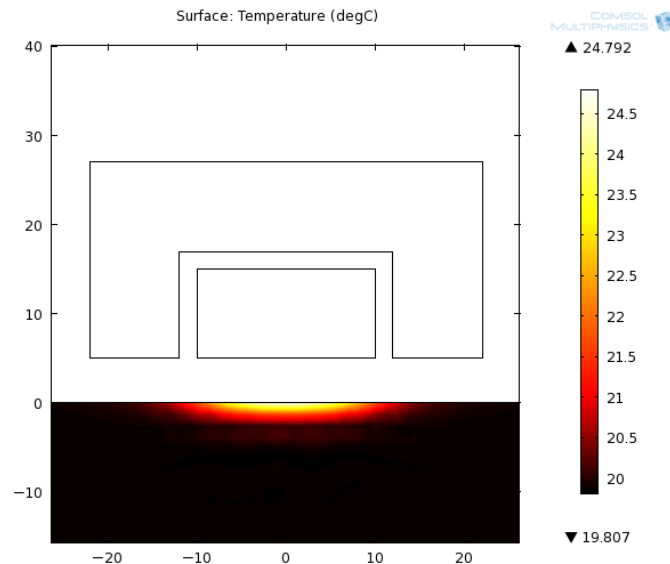


**Figure 34 The starting of heating**

Figure 35 presents the heating process accompanied with the motion, so the heating area moves to form a well distributed heating surface. The very surface has the highest temperature because of the skin effect, and the temperature of the subsurface area is also high but lowers than the surface. The subsurface heating layer is heated by heat transfer process.
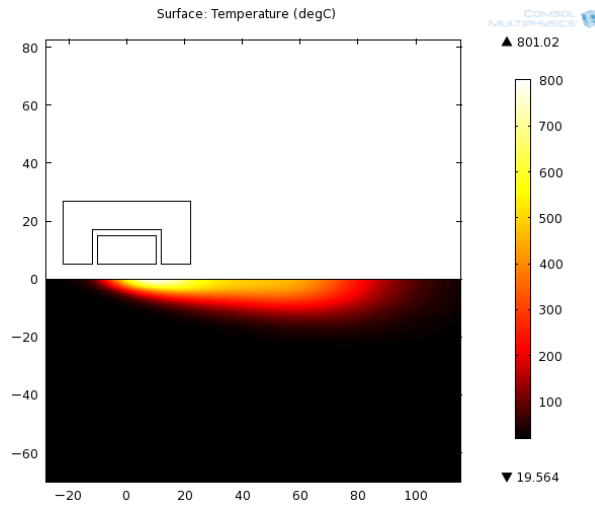
**Figure 35 The heating process with motion**

Figure 36 presents after 10s, the cooling system is applied into the system, the surface of workpiece cools down rapidly but the subsurface area is still hot because the rate of heat transfer is not as high as the coolant. In this circumstance, at the certain position and certain time, the surface is cool but the subsurface has a high temperature that can be used for further grinding to obtain superficial compressive stress.
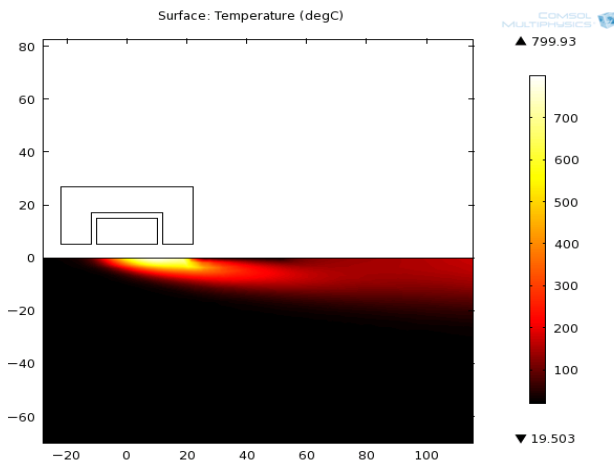


**Figure 36 Forming of subsurface heating layer**

The peak value and depth of the peak will be considered. The grinding process requires the surface of workpiece with not too high temperature because it may become soft after heating. The surface after cooling should be lower than 100℃ as preparation for grinding. Figure 37 presents the peak value of 330℃ and depth of 4.2mm.
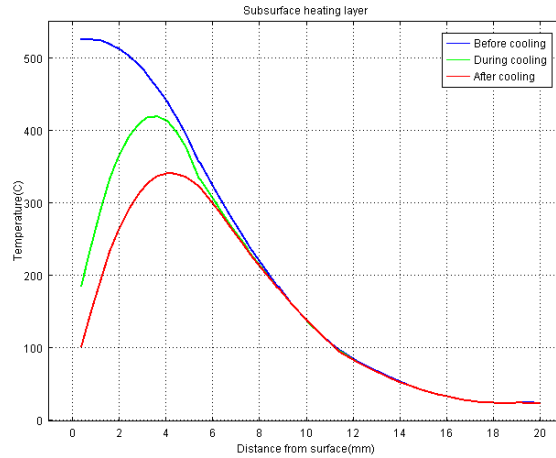
38

**Figure 37 Forming of subsurface heating layer**

In the following sections, the effects of induction current input, frequency, coolant, cooling position and feed are studied to have a comprehension understanding of the subsurface heating layer forming process. A deeper subsurface heating layer with a higher temperature is preferred to affect the distribution of the residual stress. To maintain the grinding process, the surface is required to limit the temperature so that the surface will not become soft.

### 4.3.2 The effects of induction current input on peak value and depth

The increasing of the Max heating temperature will generate a higher temperature subsurface heating layer and depth is a little deeper as Figure 38 presents. The corresponding currents input are I=730, 680, 630, 580A. f=10 kHz.
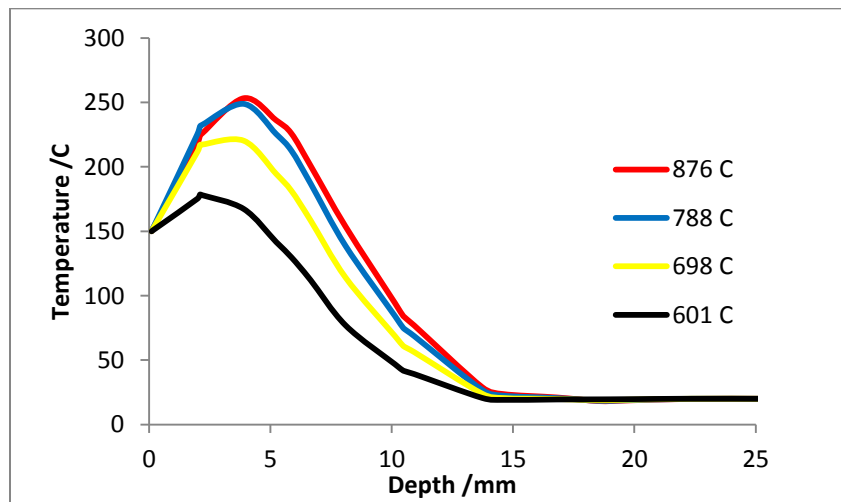


**Figure 38 Subsurface heating layer with different induction heat input**

39

From Figure 38, the subsurface heating layer can be analysis, peak depth and peak temperature are presented in Figure 39 and Figure 40. With a higher energy input, the peak depth can be lager, with a current input of 730A, the peak can be as deep as 5mm with a temperature of 250 ℃.
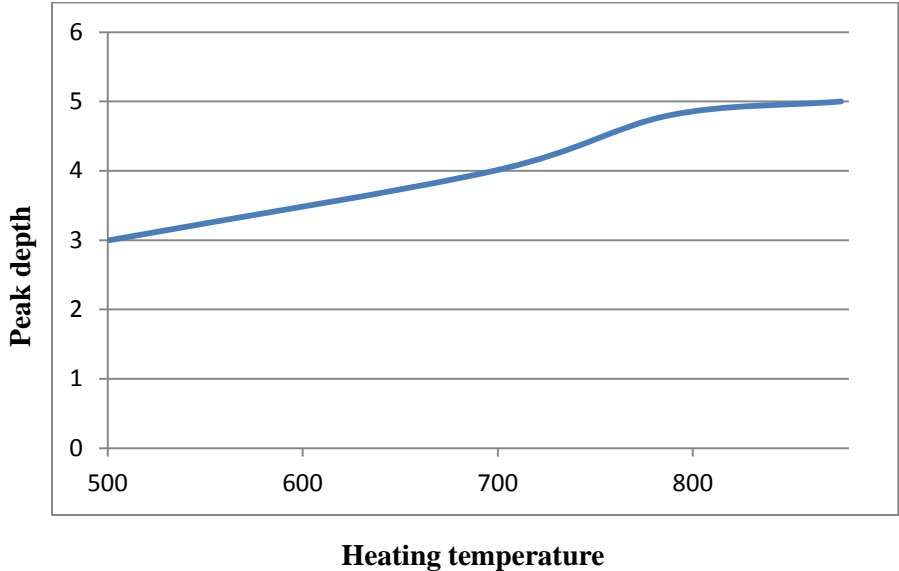


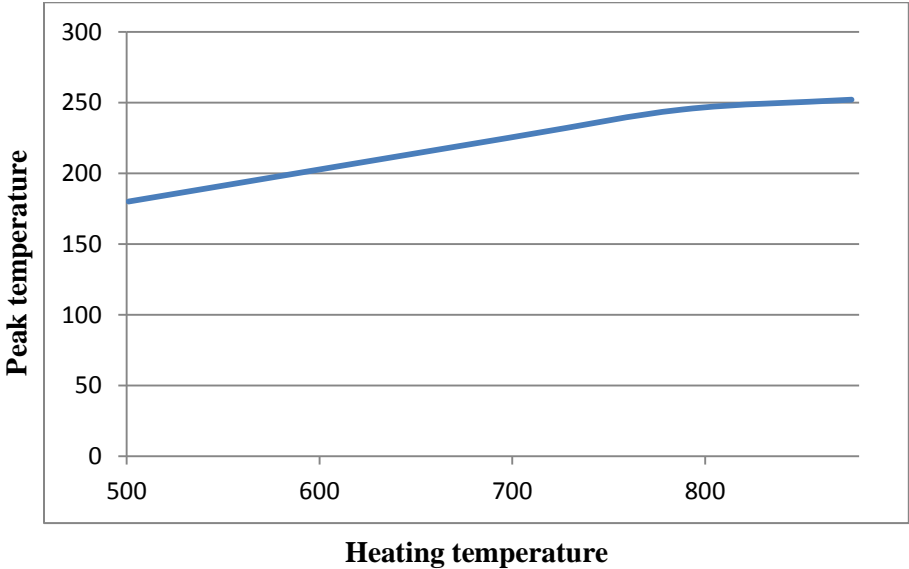**Figure 39 Peak depth of the subsurface heating layer with different induction heat input**



**Figure 40 Peak value of the subsurface heating layer with different induction heat input**

### 4.3.3 The effects of induction frequency input on peak value and depth

The increasing of the frequency will generate a shallower case depth but a higher temperature with same current value input. With the same power input, smaller frequency is better for the formation of the subsurface heating layer, comparing the Figure 41, Figure 42 and Figure 43.
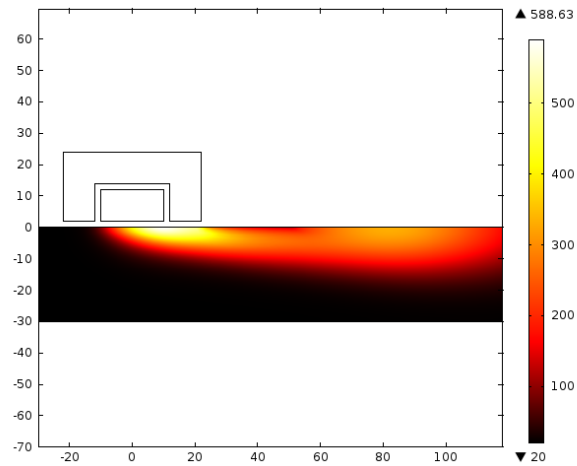


F=10k, I=600A, T$_{max}$=590℃, Skin depth=5.58mm

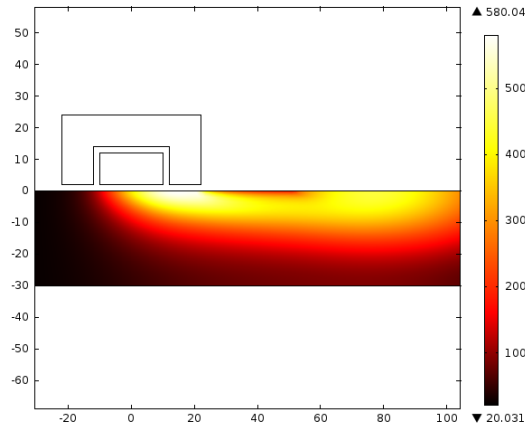**Figure 41 Temperature field with frequency input of 10kHz**

In Figure 41, with a input current of 10kHz, 600A, before cooling, the temperature can be as high as 590℃. The skin depth value is 5.58m.
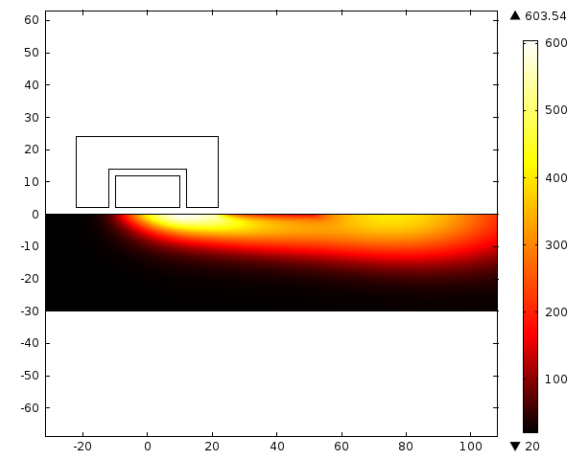


F=5k, I=840A, Tmax=600℃ Skin depth=7.89mm

**Figure 42 Temperature field with frequency input of 5kHz**

In Figure 42, the frequency reduces to 5 kHz, and skin depth increases to 7.89mm, that benefit a deeper peak value.



F=1k, I=2000A, Tmax=580℃ Skin depth=17.65 mm

**Figure 43 Temperature field with frequency input of 1kHz**

In Figure 43, the frequency continues reduces to 1 kHz, the skin depth can be as high as 17.6mm. But to maintain same temperature as a preparation for the cooling step, the current value needs to be increased to 2000A that is not recommended.
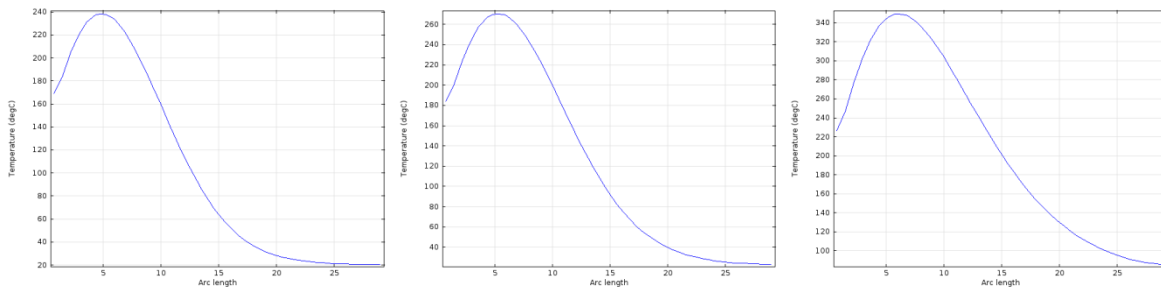


a)　Depth=5mm $T_{peak}$=240℃; b) Depth=6mm $T_{peak}$=270℃; c)Depth=7mm $T_{peak}$=350℃

**Figure 44 the subsurface heating layer with different frequency input**

Based on the figures above, Figure 44 presents the heated subsurface layer, smaller frequency current benefits on the depth of peak temperature. On the other hand, low frequency results in small energy input, to keep a fast heating rate, the current should be larger. For our induction process, the frequency should be as small as possible but keep the energy input.

### 4.3.4 The effects of coolant heat transfer coefficient on peak value and depth

The heat transfer efficient should be exceed a certain value, or the surface temperature cannot reduce under 100℃, and with water as agent, the value cannot be more than 50000 W/m2K, usually the value is around 10000 W/m2K. As the simulation result presents in Figure 45, high HTC coolant will take heat away from the surface fast, the gradient between surface and subsurface layer will be larger. On the other hand, it's also important to limit the HTC because too high a rate of cooling leads to thermal stresses in the product and consequently to cracks or fractures [19]. The peak value of the heating layer can be as high as 270℃ with a HTC value of 50000W/m2K as Figure 46 presents.
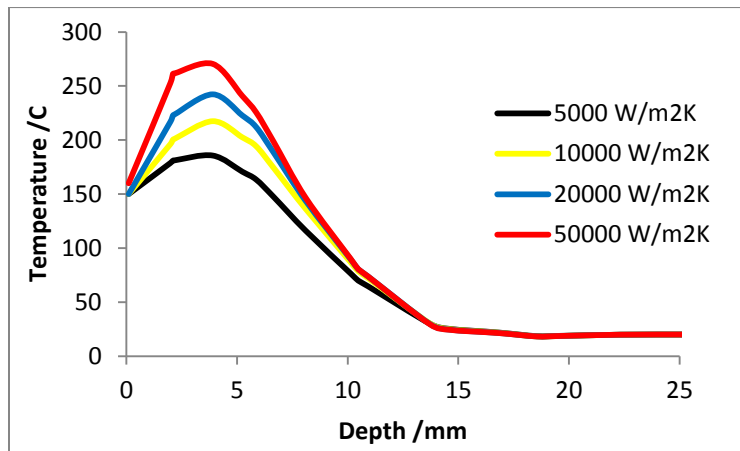


**Figure 45 Heating layer with different heat transfer efficient**

As the simulation result presents in Figure 45, the heat transfer efficient don't change the peak depth much, so does the peak value. So the heating layer cannot be modified by the parameter of heat transfer efficient.
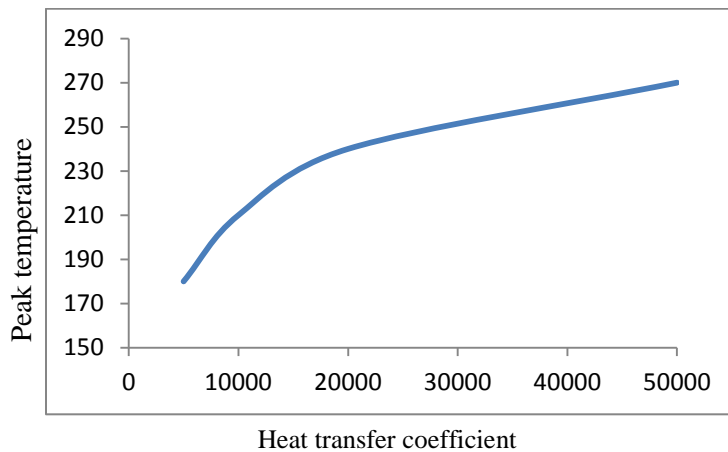


Heat transfer coefficient

**Figure 46 Effect of heat transfer efficient on peak value**

43

### 4.3.5 The effect of coolant position on peak value and depth

With proper current input and the applied coolant, a controllable subsurface layer can be formed. In the process, the distance between the coil and cooling system should also be controlled. Larger gap will increase the peak temperature while reduce the depth of peak value as Figure 47 presents.
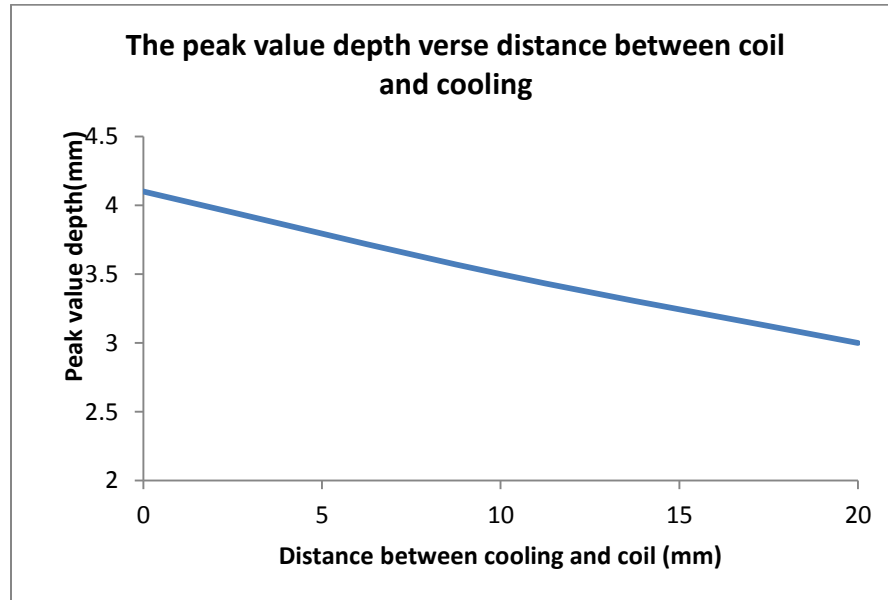


**Figure 47 The peak value depth verse distance between coil and cooling**

### 4.3.6 The effects of feed rate on peak value and depth

The feed rate will change the depth of the subsurface heating layer, as showed in the figure, higher speed will result in a smaller peak depth and peak value as presented in Figure 48. Smaller feed rate will provide more power input for certain area and benefit on the heat transfer to deeper layer. To determine the feed rate, the grinding process needs also be considered.

**Figure 48 The subsurface heating layer with different feed rate**

## 4.4 Conclusion

The finite element analysis method is applied to simulate the process of the subsurface heating layer generating. COMSOL Multphysics is selected to do the simulation. The induction phenomenon is simulated with the software including the skin effect, proximity effect and slot effect.
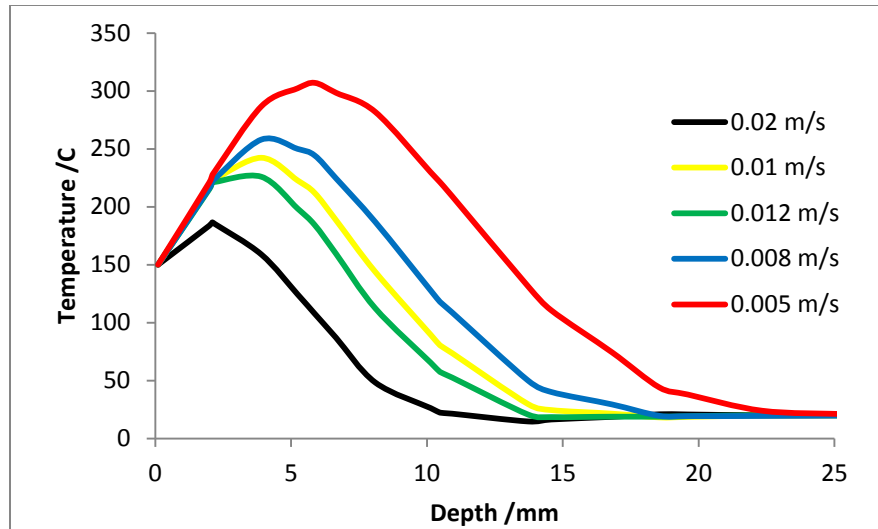
Current, frequency, feed rate, coolant heat transfer coefficient is considered to regulate the subsurface heating layer. Also the concentrator is used to concentrator the electromagnetic field and improves the heating efficiency. More energy input or smaller feed rate will benefit on a higher peak value, and larger coolant HTC and smaller feed rate will be used for a deeper layer.

With a feed rate of 0.01m/s, 10K heat transfer coefficient, 730A, 10 kHz current, subsurface with a peak value around 250C, 4mm depth can be generated

# Chapter 5.  Summery and future work

The numerical models of the subsurface heating technology are built in the thesis, and the models are realized with the finite element analysis software COMSOL, and the effects of different parameters are studied.

Skin effect, proximity effect and slot effect that will affect the performance of the induction heating. Based on the effects, concentrator is applied to improve the heating efficiency. Proper thickness, smaller gap, closer to workpiece is preferred for the concentrator to obtain the best heating function effect.

Subsurface heating layer is regulated by heating resource, feed rate, coolant and HTC. Heating effect is determined directly by the current and frequency input which also determine the peak value of the. The feed rate of the heat source and coolant HTC influence the depth of the heating layer.

The feed rate of the heat source should be well controlled to generate a moving temperature field. With cooling system, the subsurface heating layer is generated. The shape and position of the subsurface is determined by the temperature field generated by induction, the position of the cooling system, and the time delay of the grinding process. With a feed rate of 0.01m/s, 10k W/m2s heat transfer coefficient, 730A, 10 kHz current input, subsurface with a peak value around 250C, 4mm depth can be generated

The stress distribution during grinding process will be studied as following research based on the parameters from the induction heating process. The research will focus on the heat generating between the wheel and the workpiece which will change the temperature field that have been formed combining the induction and cooling process. To generate compressive stress is the objective of the research which is determined mostly by the temperature field. Simulation based on the thermal stress model of COMSOL will be applied to study the surface stress.

Suggestion for following experiment will be given based on the simulation result, including the parameters of the coil and concentrator, also the current and frequency will be applied. To implement the experiment well, the system should be well designed because the strict requirement of the delay time for different procedure to create the surface stress.

# Reference

[1] R.M. Arunachalam, M.A. Mannan, A.C. Spowage. Residual stress and surface roughness when facing age hardened Inconel 718 with CBN and ceramic cutting tools. International Journal of Machine Tools & Manufacture 44 (2004) 879–887

[2] Pei-lum Tso. Study on the grinding of Inconel 718. Journal of Materials Processing Technology 55 (1995) 421-426

[3] P.N. Moulik, H.T.Y. Yang, S. Chandrasekar. Simulation of thermal stresses due to grinding. International Journal of Mechanical Sciences 43 (2001) 831-851

[4] X. Chena, W.B. Roweb, D.F. McCormack. Analysis of the transitional temperature for tensile residual stress in grinding. Journal of Materials Processing Technology 107 (2000) 216±221

[5] Liang He, Kevin Rong. Project proposal.

[6] M. Rahman, W.K.H. Seah and T.T. Teo. The machinability of Incone1 718. Journal of materials Processing teclmology 63 (1997) 199·204

[7] S. Malkin, C. Guo. Thermal Analysis of Grinding. Annals of the CIRP Vol. 56/2/2007

[8] H. D. Merchant, G. S. Murty, S. N. Bahadur, L.T. Dwivedi, Y. Ehrotra. Hardness-temperature relationships in metals Journal of materials of (1973) 437 442

[9] W. Brian Rowe. Thermal analysis of high efficiency deep grinding. International journal of machine tools & manufacture 41 (2001) 1–19

[10] K. Sadeghipour, J.A. Dopkin, K. Li. A computer aided finite element/ experimental analysis of induction heating process of steel. Computers in Industry 28 (1996) 195-205

[11] C. Chaboudez, S. Clain, R. Glardon. Numerical modeling in induction heating for axisymmetric geometries. IEEE transactions on. VOL. 33, NO. 1. Jan1997

[12] Bogdan W. KruszynÂski, Ryszard WoÂjcik. Residual stress in grinding. Journal of materials processing technology 109 (2001) 254±257

[13] Inconel alloy 718. www.specialmetal.com

[14] Lawrence R. Egan and Edward P. Furlani. A computer simulation of an induction heating system. IEEE transactions on. VOL. 21, NO. 5. Sep 1991

[15] Stanley zinn and S. L. Semiatin. Coil design and fabrication basic design and modifications. Heat treating, June 1988

[16] H.K. Jung and C.G. Kang. An Induction heating process with coil design and solutions avoiding coarsening phenomena of Al-6 Pct Si-3 Pct Cu-0.3 Pct Mg alloy for thixoforming. Metallurgical and materials transactions A, Volume 30 November 1999—2967

[17] M. Kobayashi, T. Matsui , and Y. Murakamit. Mechanism of creation of compressive residual stress by shot peening. International Journal of Fatigue, Vol. 20, No. 5, pp. 351–357, 1998

[18] M.A.S. Torres, H.J.C. Voorwald. An evaluation of shot peening, residual stress and stress relaxation on the fatigue life of AISI 4340 steel. International Journal of Fatigue 24 (2002) 877–886

[19] M. Bamberger, B. Prinz. Determination of heat transfer coefficients during water cooling of metals. Materials Science and Technology April 1986 Vol. 2

[20] S. Sen, B. Aksakal, A. Ozel. Transient and residual thermal stresses in quenched cylindrical bodies. International Journal of Mechanical Sciences 42 (2000) 2013-2029

[21] Chen Ming, Li Xiaotian. Studies on the grinding characteristics of directionally solidified nickel-based super alloy. International Journal of Mechanical Sciences 116 (2001) 165-169

[22] M. Mahdi, L. Zhang. Applied mechanics in grinding—VI. Residual stresses and surface hardening by coupled thermo plasticity and phase transformation. International Journal of Machine Tools & Manufacture 38 (1998) 1289–1304

[23] M. Mahdi, L. Zhang. Applied mechanics in grinding –V. thermal residual stress. International Journal of Machine Tools & Manufacture 37 (1997) 619–633

[24] Shengping Wang, Yongjun Li. Compressive residual stress introduced by shot peening. Journal of Materials Processing Technology 73 (1998) 64–73

[25] K. Sadeghipour, J.A. Dopkin, K. Li. A computer aided finite element experimental analysis of induction heating process of steel. Computers in Industry 28 (1996) 195-205

[26] Hiroki Kawaguchi, Masato Enokizono. Thermal and magnetic field analysis of induction heating problems. Journal of Materials Processing Technology 161 (2005) 193–198

[27] A.D. Batako, W.B. Rowe, M.N. Morgan. Temperature measurement in high efficiency deep grinding. International Journal of Machine Tools & Manufacture 45 (2005) 1231–1245

[28] M. Mahdi, L. Zhang. The finite element thermal analysis of grinding process by ADINA. Computers & Struc/ures Vol. 56, No. Z/3, pp. 313-320, 1995

[29] Resource Guide for Induction Technology. www.fluxtrol.com.

[30] N. Biju, N. Ganesan. Frequency optimization for eddy current thermography. NDT&E International 42 (2009) 415–420

[31] E.-G. Ngl, D. W. Lee2, A. R. C. Sharmanl. High Speed Ball Nose End Milling of Inconel 718. Annals of the ClRP Vol. 49/1/2000

[32] A. Della Savia1. Induction Heating of Samples in Vacuum Systems. Excerpt from the Proceedings of the COMSOL Users Conference 2007 Grenoble

[33] Matej Kranjc, Anze Zupanic. Numerical analysis and thermography investigation of induction heating. International Journal of Heat and Mass Transfer 53 (2010) 3585–3591

[34] Nikolaos Tsopelas, Nicolaos J. Siakavellas. Influence of Some Parameters on the Effectiveness of Induction Heating. IEEE Transactions on magnetics, VOL. 44, NO. 12, Dec 2008

[35] F. Dughiero, M. Forzan. Solution of coupled electromagnetic and thermal problems in induction heating applications. Computation in Electromagnetics, 10-12 April 1996

[36] Valentin Nemkov, Robert Goldstein. Computer simulation for fundamental study and practical solutions to induction heating problems. The International Journal for Computation and Mathematics in Electrical and Electronic Engineering Vol. 22 No. 1, 2003 pp. 181-191

[37] D. Dudzinski, A. Devillez. A review of developments towards dry and high speed machining of Inconel 718 alloy. International Journal of Machine Tools & Manufacture 44 (2004) 439–456

[38] Alexander Boadi, Yuji Tsuchida.Designing of suitable construction of high-frequency induction heating coil by using finite-element method. IEEE Transactions on magnetics, Vol. 41, NO. 10, Oct 2005